Terminal Proterozoic cyanobacterial blooms and phosphogenesis documented by the Doushantuo granular phosphorites II: microbial diversity and C isotopes

Zhen-Bing She [a, b*], Paul Strother [c], Dominic Papineau [d, e]

[a] *State Key Laboratory of Biogeology and Environmental Geology, Wuhan 430074, China*

[b] *Faculty of Earth Sciences, China University of Geosciences, Wuhan 430074, China*

[c] *Department of Earth and Environmental Sciences, Boston College, Chestnut Hill, MA 02467, USA*

[d] *London Centre for Nanotechnology, University College London, London*

[e] *Department of Earth Sciences, University College London, 17-19 Gower Street, London, United Kingdom*

Abstract

An unprecedented period of phosphogenesis, along with massive deposition of black shales, major perturbations in the global carbon cycle and the rise of atmospheric oxygen, occurred in the terminal Proterozoic in the aftermath of the Marinoan glaciation. Although causal links between these processes have been postulated, evidence remains challenging. Correlated *in situ* micro-analyses of granular phosphorites from the Ediacaran Doushantuo Formation in Yichang, South China, suggested that cyanobacteria and associated extracellular polymeric substances (EPS) might have promoted aggregated granule growth and subsequent phosphatization (She et al., 2013). Here, we present new paleontological data for the Doushantuo phosphorites from Yichang, which, combined with Raman microspectroscopy and carbon isotope data, further document links between the biology of cyanobacteria and phosphogenesis. Mapping of microfossils in thin

* Corresponding author at: Faculty of Earth Sciences, China University of Geosciences, Wuhan 430074, China. Tel: +86 27 67883001.

E-mail address: zbsher@gmail.com.

section shows that most phosphatic granules contain microfossils that are dominated by colonies of *Myxococcoides*, along with several filamentous genera generally considered to represent cyanobacterial sheaths. In addition, the phosphorites and associated rocks have $\delta^{13}C_{org}$ values in the range of -26.0‰ to -29.7‰ VPDB, consistent with photoautotrophic carbon fixation with the Rubisco enzyme. Close association of phosphorites with the Marinoan tillites in stratigraphic level supports a genetic link between deglaciation and phosphogenesis, at least for the Doushantuo occurrence. Our new data suggest that major cyanobacterial blooms probably took place in the terminal Proterozoic, which might have resulted in rapid scavenging of bioavailable phosphorus and massive accumulations of organic matter (OM). Within a redox-stratified intra-shelf basin, the OM-bound phosphorus could have liberated by microbial sulfate reduction and other anaerobic metabolisms and subsequently concentrated by Fe-redox pumping below the chemocline. Upwelling of the bottom waters or upward fluctuation of the chemocline might have brought P-enriched waters to the photic zone, where it was again scavenged by cyanobacteria through their EPS to be subsequently precipitated as francolite. The feedbacks between enhanced continental weathering, cyanobacterial blooms, carbon burial, and accelerated phosphorus cycle thus controlled the marine biogeochemical changes, which led to further oxygenation of the atmosphere and oceans, ultimately paving the way for the rise of metazoans.

Keywords: Doushantuo Formation, Microfossils, Carbon isotopes, Cyanobacterial blooms, Phosphorus cycle

1. Introduction

Worldwide phosphogenic events took place in the immediate aftermath of the Neoproterozoic glaciation period, resulting in some of the largest phosphorus deposits in Asia, Australia, Africa and South America (Cook, 1992; Cook and Shergold, 1984). As phosphorus is an essential nutrient and an important driving and regulating force behind biological productivity (Redfield,

1958; Föllmi, 1996), massive deposition of phosphate is generally related to biological accumulation of excess phosphorous. Models have suggested that enhanced post-glacial weathering might have led to blooms of primary producers in the oceans (Kirschvink et al., 2000), which in turn would have promoted phosphogenesis (Papineau, 2010). Direct links between biological activity and phosphogenesis have long been proposed (Föllmi, 1996, and references therein). Sulfur isotopes of framboidal pyrite and organic biomarkers from modern phosphorites have documented the importance of bacterial sulfate reduction in the formation of modern phosphatic sediments from the Peruvian and California coast (Arning et al., 2009; Berndmeyer et al., 2012). Other studies have shown that sulfur-oxidizing bacteria can release orthophosphate into pore waters where it accumulates and rapidly precipitated as apatite (e.g., Schulz & Schulz, 2005; Goldhammer et al., 2010; Brock & Schulz-Vogt, 2011). Cyanobacteria have not been specifically targeted in studies of phosphogenesis despite the fact that primary production in today's oceans is provided by a consortium of eukaryotic microalgae and cyanobacteria.

The Doushantuo Formation (ca. 635–551 Ma) in South China is well known because it contains exceptionally well-preserved fossil evidence for putative earliest embryos (Xiao et al., 1998; Chen et al., 2004), which have been variably interpreted as thiomargarita-like sulfur bacteria (Bailey et al., 2007), as algae (Xue et al., 1999) and as encysting protists (Huldtgren et al., 2011). Adult metazoans (Zhu et al., 2008), multicellular algae and acanthomorph acritarchs have also been reported (Xiao, 2004; Xiao et al., 2004, 2014; Yin et al., 2007). Moreover, the Doushantuo Formation preserves a chemostratigraphic record of significant perturbations of the carbon and sulfur cycles that correlate with global tectonic and climate changes and oxygenation of the atmosphere and the oceans (Och and Shields-Zhou, 2012, and references therein). Thus, the Doushantuo Formation presents a unique window for understanding feedbacks between global chemical changes and biological evolution at the dawn of animal life. While the evolution of

metazoans has been the focus of most studies, the biogeochemical significance of other organisms, including primary producers, has received less attention. The prior recognition of abundant well preserved in situ microfossils from the Doushantuo phosphorites (Zhongying, 1985; Zhou et al., 2005; She et al., 2013) hints at an intimate relation between primary phosphatization and fossilization of microorganisms. In a recent study, we suggested that cyanobacteria and associated extracellular polymeric substances (EPS) might have promoted accretionary granule growth and provided nucleation sites for rapid crystallization of apatite in the Doushantuo environment (She et al., 2013). Now, we present results of detailed systematic mapping of microfossils in thin section and Raman microspectroscopy and carbon isotope data which suggest that, while other microorganisms such as sulfur bacteria may have played a role in phosphogenesis, cyanobacteria also played important roles in phosphorus cycling and phosphogenesis. This study favors a biological origin for the Doushantuo phosphorites and suggests links between biology, the changing environment, and phosphogenesis at this critical time of Earth history.

2. Sample description

Samples of black shales and phosphorites (designated with prefix "TP", Fig. 1) were collected from and near major phosphorus-bearing horizons in the Doushantuo Formation (member II) in the Taopinghe mining area, north of Yichang City (Fig. 1a and b in She et al., 2013). The phosphorus-bearing sequence overlies basal, cap dolostones. It is characterized by interbedded black potassic shale and phosphorite with gradual increasing dolostones upsection (Fig. 1c in She et al., 2013). The phosphorites are mostly black to brownish banded rocks with granular textures that are visible to the naked eye. When observed with a petrographic microscope, individual granules display distinct oncoid-like zoning. They are composed primarily of cryptocrystalline apatite although minor microcrystalline apatite, quartz and carbonate minerals are present as cement or later replacement (She et al., 2013).

Another cherty dolomicrite sample (YG0914, Fig. 1) was collected from the uppermost of cap carbonate (member I) of the Doushantuo Formation near Liantuo Village (GPS coordinates: 30°51'12.5"N, 111°09'11.5"E), ~20 km NW of Yichang. The sample is mainly composed of dolomicrite and is generally brownish grey to dark grey. Black chert nodules are common in this horizon and are often rimmed by brownish "rusted" dolomicrite. There appears to be some chaotic layering in the dolomite matrix which roughly encompass the chert nodules (Fig. 1) that points to an early diagenetic origin for the chert.

According to previously published data, the age of the studied section is constrained to be between 635 and 614 Ma (Condon et al., 2005; Liu et al., 2009), corresponding to the first 20 Myr of the Ediacaran Period. Paleogeographic reconstructions show that the majority of the Doushantuo Formation in the Yangtze platform (the NW part of the South China Craton) was deposited in a restricted basin on a rimmed carbonate shelf (Jiang et al., 2011). Sedimentological and petrographic data have shown that the Yichang phosphorites and black shales were deposited in relatively low energy, shallow water settings (Zhou et al., 2005; She et al., 2013).

3. Methods

3.1 Petrography and documentation of microfossils

Observation and documentation of polished thin sections were performed with an Olympus BX51 optical microscope equipped with a mechanical stage. Identification of microfossils was based on morphological criteria including shape, size and wall structure. For all examined thin sections, important targets including interesting textures and microfossils were documented with exact locations marked on maps of the thin sections and pictures taken for each at 40X, 100X, 400X and 1000X magnifications. Systematic documentation of microfossils in thin section TP0901S was conducted by scanning along linear vertical (Y axis) transects across the thin section at 400X magnification. Each successive transect was separated by displacing the slide

~200 µm along the X axis of the microscope stage, which provide a complete cover of the examined area. Occurrences of different microfossils were marked on the map by different shapes or colors, with pictures taken for each (1379 photos generated). Size frequency distributions of coccoidal microfossils were obtained by measuring the diameters of 15 to 20 cells for well-preserved colonies in five thin sections. Immersion oil was used only on one thin section for high resolution imaging after Raman micro-spectroscopy.

3.2 Raman micro-spectroscopy

Confocal laser Raman micro-spectroscopy was performed with a WITec alpha 300R system equipped with a 532 nm laser with output power maintained at ~5 mW. Raman hyperspectral scans were performed under a 100X objective (N.A. = 0.9) with a 50µm diameter optic fiber and collected on a Peltier-cooled EMCCD detector. Spatial resolution was ~360 nm/pixel and spectral resolution was ~0.1 cm^{-1}. Individual spectra shown in this work represent averages of selected regions with similar spectral characteristics. Detailed descriptions of this method can be found in Bernard et al. (2008). Raman hyperspectral analyses were performed 3-10 microns below the thin section surface, therefore ruling out potential artifacts induced by polishing or surface contamination. Raman spectra of different minerals were compared with spectra from the online database http://rruff.info/.

3.3 Isotope Ratio Mass Spectrometry

Slabs of phosphorite and black shale were polished with silicon carbide paper and then cleaned by ultrasonication, repeatedly rinsed with deionized distilled water and dried. Slabs were stored in Al foil pre-muffled at 600 ^{o}C for 2 hours until analysis. They were then micro-drilled with a 2.0 mm diameter SiC drill bit in areas with the fewest pores and cracks to obtain pristine rock powders (Fig. 1). For carbon isotope analyses of total carbon (TC), 3-5 mg of whole-rock powders were weighed in Ag capsules pre-muffled at 600 ℃ for 2 hours. For carbon isotope

analyses of total organic carbon (TOC), 10-25 mg of powders were gently acidified in Ag capsules using ultrapure 6N HCl (Sequanal Grade, Thermal Scientific) to remove carbonate minerals.

Carbon isotope analyses were performed with an ECS 4010 elemental analyzer (EA) linked to a ThermoFisher Delta V Plus IRMS through a Conflo III interface as previously described (Papineau et al., 2010). $\delta^{13}C$ values are reported as per mil (‰) deviation from V-PDB. Uncertainties determined by multiple measurements of NBS-22, USGS-40 and USGS-41 were better than 0.10‰ (1σ, n = 27), 0.14‰ (1σ, n = 14) and 0.37‰ (1σ, n = 8), respectively. Analyses of 0.13 to 0.20 mg of organic carbon from a compositionally similar standard (Peru mud; $\delta^{13}C_{org}$ = -19.95‰, TOC = 6.7%wt) gave a 1σ reproducibility better than ±0.3 ‰ (n = 5) for $\delta^{13}C$ and ±1.1% (n = 5) for total organic carbon (TOC). Muffled Ag boats contained less carbon than the detection limit (Papineau et al., 2011).

4. Results

4.1 Abundance and systematic petrographic mapping of microfossils

Microfossils were identified on the basis that they are, 1) morphologically congruent with cellular microorganisms, 2) diverse in mode of occurrence, 3) organic-walled, and 4) directly comparable to previously reported microfossils. The main morphological categories include spheroidal to ellipsoidal unicells and colonies, non-septate filaments (tubes), septate filaments, and coiled filaments. Microfossils occur almost exclusively within the medium sand-sized granules except that thin filaments (width < 0.5 μm) occasionally are present in the inter-granular cement. Although microfossils are abundantly preserved in the Doushantuo granular phosphorites, their quality of preservation varies considerably. In many microfossils fine structural details are preserved while others are obscured by degradation.

Thin section TP0901S, with exceptionally well-preserved microfossils, was systematically mapped to determine if mat fabrics were structurally preserved and to statistically characterize different morphotypes. Mapping of microfossils yielded a density of ~300 recognizable colonies (each colony counted as one) or solitary microfossil per cm^2 (in a standard 30 μm thin section) (Fig. 2). Colonial *Myxococcoides* (Fig. 3), including both relatively well-preserved and degraded forms, accounted for 50% of approximately 700 counted occurrences (Table 1, Fig. 4). As *Myxococcoides* is exclusively colonial, this percentage represents the minimum relative abundance. Less abundant taxa include, in descending order of abundance (occurrence), degraded filaments (18.5%), *Eomycetopsis* (8.3%), *Gunflintia* (7.2%), *Obruchevella* (6.4%), possible green algae (4.7%) and unnamed thin filaments (width < 0.5μm, 2.0%) (Table 1, Fig. 4). Rare occurrence of *Eoentophysalis* (1.9%), *Heliconema* (0.7%), and *Gloeodiniopsis* (0.7%) were also observed. In general, microfossils appear to be randomly distributed in the plane of the thin section (Fig. 2). The exception to this general impression occurs near cracks where post-depositional alteration has removed any recognizable microfossils. The generally uniform distribution of all microfossil types in the thin section also suggests their pelagic provenance from the water column, as opposed to them being of benthic origin, where microbial mat type layering would be expected. There is indication for bacterial cells that actively induce biomineralization may be preferentially preserved (Couradeau et al., 2012; Cosmidis et al., 2013) so the microbial community composition that we report here may not necessarily reflect an accurate picture of the original microbial community composition. Furthermore, the microbial community composition is likely to have evolved from sedimentation through the various stages of diagenesis.

4.1.1 Spheroidal microfossils

Myxococcoides. *Myxococcoides* is the dominant taxon in the examined slides (Fig. 2 and Fig. 3) commonly forming dense clusters set in a matrix of cryptocrystalline apatite and finely disseminated organic matter (She et al., 2013). The colonies, with diameters generally around 50

μm and sometimes up to 200 μm, may comprise a few to hundreds of single-walled spheroidal individuals (Fig. 3 a-b). Measurements of over 400 cell diameters ranged from 4 to 13 μm, with a mean of 7.5 μm (σ =1.5) (Fig. 4b). This represents the typical 2-D projections of these 3-D cells cut in a range of 2-D planes and directions. Thickness of the cell walls is around 0.5-1.0 μm. Neither enclosing sheath nor internal structures were observed. Cells appear to be geometrically unordered. Possibly dividing cells were occasionally observed (Fig. 3c). These resemble *Myxococcoides minor* as reported from the Bitter Springs Formation of Central Australia (Schopf, 1968), the Belcher Group of Canada (Hofmann, 1976), the Kheinjua Formation of Northern India (Kumar and Srivastava, 1995), and the Chichkan Formation of South Kazakhstan (Fig. 3d) (Sergeev and Schopf, 2010).

Eoentophysalis. Encapsulated colonial spheroids are rare in the Yichang phosphorites. They are characterized by "pigmented" spheroids (cell-like units) encapsulated in relatively thick envelope (Fig. 5a-d). The spheroids may be solitary, in pairs (Fig. 5b and c), in tetrads (Fig. 5d), or in irregular clusters. The cell-like units are spheroidal, ellipsoidal, or subpolyhedral and are 10 to 15 μm across, similar to the material described from the Chichkan Formation in Kazakhstan by Sergeev and Schopf (2010). Envelopes are generally around 2 μm in thickness, and multi-laminated textures are occasionally visible (Fig. 5b).

Gloeodiniopsis. Only a few occurrences were observed for this taxon. The spheroidal cells are solitary, and encompassed by a thick, prominent, distinctly laminated sheath (Fig. 5e). The cells are approximately 6 μm in diameter, and the surrounding sheath is 4 μm in thickness. Dark organic matter occupies almost the entire internal space of the cells, whereas the enclosing sheaths are pinkish yellow and are composed of 4 to 5 concentric layers of uncertain composition. A fuzzy outer envelope is vaguely visible in some specimens. These microfossils closely resemble the species *Gloeodiniopsis lamellosa* reported in Schopf (1968).

4.1.2 Filamentous microfossils

Relatively well preserved specimens include non-septate *Eomycetopsis* and *Gunflintia*, the helically coiled filaments *Obruchevella* and *Heliconema*, a possible green alga, and *Microcoleus*-like filaments (Fig. 6). Other more degraded filaments precluded taxonomic assignment (e.g., Fig. 7g).

Eomycetopsis. *Eomycetopsis* forms non-septate filaments that are generally 2-5 µm in width and can be straight to moderately sinuous, occasionally forming intertwined populations. The majority of elongate phosphate granules contain *Eomycetopsis* (Fig. 6a), and these appear to represent microbial mat fragments. In other cases, however, they tend to colonize around clusters of feldspars or inner cores of phosphate granules (She et al., 2013), reflecting what seems to be accretionary growth of granules which were in the water column. Most commonly, *Eomycetopsis* occurs together in mixed populations of coccoids or septate filaments in the same granules.

Gunflintia. These filaments (tubes) are slender, unbranched, and commonly slightly curved. They can be over 100 µm long and 0.5-1.5 µm across (Fig. 6b). Although many appear to be septate, apparent crosswalls are mostly likely degradational artifacts. These specimens are similar to *Gunflintia minuta* as reported from the Gunflint Formation (Barghoorn and Tyler, 1965; Strother and Tobin, 1987), the Duck Creek Formation (Knoll et al., 1988), and elsewhere in the Doushantuo Formation (Zhongying, 1982). *Gunflintia* is the only taxon that occurs not only in the granules but in the inter-granular cement as well. The microfossils may appear to be aligned concentrically or randomly inside the granules. Others are clearly parallel to or penetrate the laminae of early diagenetic cement (Fig. 6c). Such populations appear to represent a later generation of microorganisms that were actively growing during early diagenesis.

Coiled filaments *Obruchevella* and *Heliconema*. Helically coiled filaments resembling extant *Spirulina* were frequently observed (Fig. 6d and e). They may be solitary or form clusters. The

filaments are tube-like and coil around an open-center that forms closely adjoining whorls. The cross section of the tube is round, 2-3 μm in diameter (Fig. 6e). The coiled structure is 5-10 μm in diameter. Filaments are non-septate, with smooth or slightly granular surface texture. The long axes of the coils are straight or slightly bent. They are assigned as *Obruchevella*, a well-known cyanobacterial genus in the Neoproterozoic-Cambrian phosphorite deposits of India, China and Russia (Sergeev and Schopf, 2010). Another type of coiled filament distinguished from *Obruchevella* by its loosely adjoining whorls can be assigned to *Heliconema* (Fig. 6f).

Possible green algae. These uniseriate filaments are generally more degraded than their non-septate counterparts. Cells are cylindrical, 27-36 μm long and 10-13 μm across. They are characterized by a three layered structure, a thin but prominent, and brown colored crust (cell wall), a thick colorless mantle, and an irregular black core that might represent residue of degraded or collapsed cytoplasm (Fig. 6g and h). We consider them to be chlorophytes, although other simple filamentous eukaryotic algae (e.g. Xanthophyta, brown algae) cannot be ruled out.

Microcoleus-like filaments. In the cherty dolomicrite sample YG0914, unlike in the phosphorites, only a few filamentous microfossils were observed. Here, filaments commonly occur as interconnected bundles. Individual trichomes are 8-10 μm in diameter and appear to be multi-laminated (Fig. 6i). Both longitudinal and transverse sections were observed. Fig. 6i shows a transverse section of a bundle of filaments, which are connected with neighboring filaments by very thin "strings". These resemble the filament bundles reported by Awramik (1985) from the Doushantuo Formation in the Yangtze Gorges. They bear some similarity to the extant oscillatoriacean cyanobacterium *Microcoleus*.

4.2 State of preservation

The Doushantuo Formation in South China, as a whole, is known to be nearly unmetamorphosed or locally experienced only lower greenschist facies metamorphism. The very low crystallinity of the phosphorites (She et al., 2013) and the preservation of abundant microfossils in varying states of apparent decay, attest as well to the low grade thermal evolution of the studied samples. This is consistent with an estimated maximum burial depth of 4 km (Jiang et al., 2006; Bristow et al., 2009) and maximum peak metamorphic temperatures of 220℃ - 360℃ calculated using Raman thermometry (She et al., 2013). As shown in our previous study, the phosphorites likely experienced a complex diagenetic history including syngenetic phosphatization, microbial sulfate reduction, albitization, silicification and later carbonatization (She et al., 2013).

Microfossils are generally poorly preserved, although exceptionally well preserved individuals are were observed. Degraded microfossils reflect both structural modification and compositional alteration. It is known that diagenetic alteration does not alter all fossils to the same degree (e.g., Knoll et al., 1988). In the Doushantuo samples, the best preserved microfossils, which retain fine structural details, appear to be brown or dark brown (Fig. 3b, Fig. 6e and Fig. 7a), a color similar to but darker than that of the enclosing phosphatic matrix. More degraded specimens, however, can be yellow, black, or opaque (Fig. 7b-d, f and g). Cells of *Myxococcoides* are commonly degraded, producing an array of degradational variants with similar textures, cell diameters, and colony sizes (Fig. 7b-e). As morphologically simple spheroids, *Myxococcoides* is not significantly affected by condensation. Rather, these microfossils were modified by migration and diffusion of organic matter that almost obliterated original textures and produced organic halos around the cells (Fig. 7b and c). For larger microfossils, however, granularization (Fig. 5a, Fig. 7g) and condensation (Fig. 6g) are more common. Compositional changes were mainly caused by thermal maturation and replacement (e.g., pyritization, Fig. 7d and e).

The various states of preservation were further documented by Raman micro-spectroscopy (Fig. 8). Well preserved microfossils in the phosphorites show distinct carbonaceous cell walls or sheath embedded in cryptocrystalline apatite (Fig. 8a and b), whereas degraded specimens display only partially preserved cell structures (Fig. 8c and e). The presence of prominent but broad D-bands (disordered carbonaceous material, near 1350 cm^{-1}, FWHM= 98-135 cm^{-1}) in the Raman spectra (spectra 1-3 in Fig. 8g, Table 2) confirms the overall low degree of thermal maturation of the organic matter. The G-bands (around 1600 cm^{-1}, FWHM= 73-86 cm^{-1}) display comparable intensities to the D-bands but with narrower peaks. The data also revealed compositional alteration of microfossils. For instance, pyritization of *Myxococcoides* and *Obruchevella* are clearly shown on the Raman hyperspectral maps (She et al., 2013). In Figure 8d, the interior of the coiled filament *Obruchevella* is of undetermined composition, as indicated by the absence of a Raman signal, although it appears to contain abundant carbonaceous material under transmitted light (Fig. 6d). In general, microfossils embedded in phosphate matrix have "noisy" Raman spectra and the peaks often bifurcate or multifurcate, probably due to structural degradation and modification of the molecular structure of the organic matter.

Microfossils preserved in chert (Fig. 6i and Fig. 8f) near base of the studied section (YG0914, Fig. 1c in She et al., 2013), however, display a distinct spectrum from those encased in phosphate, which is characterized by sharp and intense G-bands and broader D-bands (spectrum 4 in Fig. 8g). The D-bands are centered around 1350 cm^{-1} (FWHM = 133 cm^{-1}) and are generally bimodal with peaks at 1338 cm^{-1} and 1357 cm^{-1}. A shoulder is present on the low wave number side of the D-band. The G-bands are slightly asymmetric and centered around 1613 cm^{-1} (FWHM = 34 cm^{-1}, Table 2). These features are similar to microfossils from the Bitter Springs Formation (spectrum 5 in Fig. 8g), the Gunflint Chert and the Chichkan Formation (Schopf et al., 2005). Given that both phosphate and chert-embedded microfossils are preserved together in the same formation, the distinct Raman signature likely reflects a taphonomically-induced difference of preservation.

Both silicification and phosphatization are capable of preservation at a cellular and subcellular level (e.g., Schopf, 1968; Battison and Brasier, 2012). Given the low thermal maturity of the Doushantuo phosphorites, along with early phosphatization, one might expect a better overall preservational level. The varying degrees of preservation witnessed in our samples, suggest that microbial remains were subject to varying degrees of decomposition before permineralization. This is consistent with the occurrence of early microbial sulfate reduction (She et al., 2013).

4.3 Distribution patterns of microorganisms

Petrographic observations demonstrate that almost all microfossils occur exclusively within phosphatic granules. Three types of granules can be described, based on their dominant microfossil content: coccoid-dominated, filament-dominated, and mixed (Fig. 9).

4.3.1 Coccoid-dominated granules

Populations of coccoids, mostly *Myxococcoides*, occupy considerable space within this granule type (Fig. 9a and b), which accounts for >60% of all documented granules. A single granule may contain more than 7 colonies of *Myxococcoides*, each of which consists of tens to hundreds of cells (Fig. 9a, arrows). The presence of multiple colonies within a single granule appears to be caused either by coalescence of different communities during growth or by disintegration of a single colony. In Fig. 9b, a population of *Myxococcoides*, which contains more than 1,000 cells, accounts for 70% of the total area of its host granule. The colonies may be located in the core or near the periphery of granules. In many cases, the distribution of coccoids coincides with an apparent organic zonation of the granule itself (Fig. 9a-b).

4.3.2 Filament-dominated granules

Filament-dominated granules are far less common (< 20% of total) than the coccoid-dominated ones. Two kinds of granules were observed. The first is characterized by concentric or asymmetrically zoned distributions of filamentous microfossils, typically *Eomycetopsis* (Fig. 9c-d). In this case, tangentially oriented and nearly radially oriented filaments form alternating zones, imparting a distinct zonation to these granules (Fig. 9c-d). These textures are similar to microfossiliferous coated grains reported from the Deoban Limestone in Lesser Himalaya (Srivastava, 2006). This alternation of distinctly oriented filaments is a fundamental characteristic of stromatolitic textures (Monty, 1976; Walter et al., 1976), attesting to the probable phototactic nature of the microbes which grew in the developing granules. The concentric texture of most granules parallels that seen in oncolites and oölites which form dynamically in the water column. They are distinctly unlike the patterns expected in a stable, benthic microbial mat, consistent with an accretionary growth model (She et al., 2013).

The second filament-dominated type of granule consists of abundant intertwining populations of (mainly) *Eomycetopsis* (Fig. 9e). In this type of granule, which has only a few occurrences per thin section, *Myxococcoides* is either entirely absent or much less abundant than in the coccoid-dominated granules. These granules are often elongate or irregular in shape. This combination of irregular gross shape with abundantly preserved internal filaments, leads to the suggestion that this type of granule represents allochthonous remains of fragmented microbial mats.

4.3.3 Mixed granules

In some granules, both coccoidal and filamentous microfossils are present. Fig. 9f shows a granule that contains a core of *Eoentophysalis* surrounded by a mantle of *Eomycetopsis*. Cells of *Eoentophysalis* are around 5 µm in diameter and characterized by irregular black bodies enclosed in 1-µm-thick clear envelopes (Fig. 9g, triangles). They form a large colony that occupies the entire core of the granule, suggesting that this colony was syngenetic with granule formation This

core, in turn, is enclosed in a mantle composed entirely of *Eomycetopsis*. The mantle, which is from 16 to 68 μm thick, is somewhat darker than the core, expressing the retention of more preserved organic matter. Orientation of the filaments is mainly tangential but in the outmost part of the mantle many tend to be radially aligned. However, this kind of regular pattern is not especially characteristic of the mixed granules. Various types of filaments (Fig. 9h, arrows) and colonies of coccoids (Fig. 9h, triangles) most often appear to be randomly distributed within the same granules. Nevertheless, these granules also display clear zonation, which implies they grew through the successive accretion of microbial communities in the water column or in the accumulating and progressively mineralizing phosphatic ooze on the local seafloor (She et al., 2013).

4.4 Carbon isotopes

As shown in Table 3 and Fig. 1, the Doushantuo phosphorites have relatively low total organic carbon (TOC) ranging between 0.02 and 0.14 wt%. $\delta^{13}C_{org}$ values of 5 samples (TP0901, TP0902, TP0903, TP0908 and TP0909) vary from -26.0 to -29.1 ‰ VPDB. Black shale and phosphatic nodule therein contain 0.93 to 1.15 wt% TOC and have $\delta^{13}C_{org}$ values of -29.7 to -28.6 ‰. Analyses of powders micro-drilled from different areas in a chert-bearing organic-rich dolomicrite (YG0914) near the top of the first member of Doushantuo Formation yielded TOC of 0.37 to 1.04 wt% and variable carbon isotopic compositions. One chert nodule (YG0914.a) has the lightest $\delta^{13}C_{org}$ of -32.9 ‰, whereas samples of dolomicrite matrix (YG0914.b and d-g) possess relatively heavier and consistent $\delta^{13}C_{org}$ values ranging from –28.5 ‰ to -26.5‰. Among these, two samples drilled from CM- rich black areas (YG0914.f and g) in the dolomicrite yielded much higher TOC of 0.78 to 1.04 wt% but similar $\delta^{13}C_{org}$ ranging between -28.2 and -26.8‰.

Total carbon contents of the phosphorites, dolomicrite and the chert nodule are 0.61 to 0.83 wt%, 3.53 to 6.67 wt% and 0.49 wt%, and $\delta^{13}C$ values of total carbon (TC) are -10.0 to -9.8‰,

+1.1 to -3.7‰, and -5.7‰, respectively. Calculated $\delta^{13}C$ of inorganic carbon (IC) are -8.5 to -6.3‰ for granular phosphorites TP0901 and TP0902. As no carbonate minerals were detected using both optical microscopy and Raman spectroscopy for the two samples, the inorganic carbon might largely represent structurally-bound carbonate in apatite. These calculated $\delta^{13}C_{IC}$ values are similar to those of authigenic phosphorites from the Phosphoria Formation in North America and in modern deposits in Namibia (McArthur et al., 1980). $\delta^{13}C_{IC}$ values for the dolomicrite sample YG0914.d-g, however, are much heavier and range from +6.6 to +7.4‰.

5. Discussion

5.1 Taxonomic affinity of the Doushantuo microfossils

The genus *Myxococcoides* was erected by Schopf (1968) to accommodate simple spheroids without inclusions. Schopf (1968) considered *Myxococcoides* to belong to the Chroococcaceae. Subsequent authors have treated this genus as *incertae sedis*, citing (relative) large cell size and lack of evidence of *in situ* division as evidence for its planktonic habit, a characteristic more often associated with eukaryotes (Knoll, 1982). As Allison and Awramik (1989) point out however, neither cell size nor the lack of evidence for cell division is conclusive for eukaryotic affinity. Unlike the Draken *Myxococcoides* reported by Knoll (1982), the size range of the Yichang specimens (4 - 13 μm in diameters) is much smaller, falling well within the size range of typical cyanobacteria. Moreover, cell division was occasionally observed within the colonies of *Myxococcoides* (Fig. 3c), which is consistent with the preservation of an actively growing colony. Battison and Brasier (2012) described eight morphotypes of microfossils, including *Myxococcoides*-like clusters, from lacustrine phosphate of the ~1.0 Ga Torridon Group, NW Scotland, but these authors cautiously made no taxonomic assignment.

Although, in general, it is not possible to place *Myxococcoides* unequivocally in the cyanobacteria, most of the other major taxa of the Yichang assemblage (*Eomycetopsis*,

Eoentophysalis and *Obruchevella*) are universally considered to belong to the cyanobacteria. *Eoentophysalis* is a common taxon in Paleoproterozoic strata (e.g., Hofmann, 1976; Sharma and Sergeev, 2004) but occurs only as scattered colonies in Neoproterozoic assemblages that are dominated by other organisms (Knoll et al., 1991). Although typically interpreted as mat-builder, the high polymorphism of *Eoentophysalis* colonies and very complicated life cycle (Hofmann, 1976) suggests that these organisms probably occupied a range of habitats *Eomycetopsis* was clearly an important microbial mat-builder (Knoll, 1982). The helically coiled fossil *Obruchevella* is well known in the Neoproterozoic-Cambrian phosphorite deposits of India, China and Russia (Sharma and Shukla, 2009). The specimens described in this study are similar to *Obruchevella exilis* (Sergeev and Schopf, 2010), a distinctive spirally coiled oscillatoriacean cyanobacterium 2.0 to 3.0 μm in diameter that resembles modern *Spirulina*.

The cyanobacterial affinity of most of the Doushantuo microfossils is also supported by carbon isotopic data. The microfossiliferous phosphorites themselves and associated black shales and dolomicrites all have $\delta^{13}C_{org}$ values in the range of -26.0‰ to -29.7‰ VPDB, which is consistent with photoautotrophic carbon fixation via the Calvin cycle, that is, fixation by the enzyme ribulose biphosphate carboxylase (Rubisco) (House et al., 2000). Although $\delta^{13}C$ values ranging from -20 to -35‰ alone do not demonstrate definitively that the associated organisms fixed carbon via the Calvin Cycle (Fuchs et al., 1979; Schidlowski et al., 1983), carbon isotope data in combination with 1) morphology-based taxonomy, 2) microbial community composition, and 3) the phosphatic sedimentary environment, suggest that the fossil organisms fixed carbon by Rubisco and are most likely cyanobacteria.

5.2 A post-glacial cyanobacteria-dominated ecosystem

The Doushantuo granular phosphorites provide us with a glimpse of the shallow marine living world following soon after the Marinoan glaciation. Microfossil assemblages of the phosphorites are dominated by abundant structurally simple coccoids (i.e., *Myxococcoides*). This

observation is consistent with the paleontological study in the Zhangcunping phosphorus mine, 9 km NW of Taopinghe, which contain abundant *Archaeophycus venustus*, a dominant coccoid form (Zhou et al., 2005). Despite its relatively large size (10-30 μm in diameter), *Archaeophycus venustus* was assigned to the *Chroococcacea* (Zhou et al., 2004; Zhou et al., 2005)).

Studies of the Doushantuo Formation from other localities in South China, however, have shown that coccoidal cyanobacteria are generally less abundant than filamentous, sphaeromorph acritarchs and multicellular algae (Awramik et al., 1985; Yuan et al., 1993; Yin and Sun, 1994; Xiao et al., 1998; Yin et al., 2007; Liu et al., 2009; McFadden et al., 2009). Although Xiao et al. (2004) noted the general similarity in biodiversity between the silicified assemblage in Doushantuo Formation in the Yangtze Gorges area and the phosphatized assemblage at Weng'an and elsewhere in South China, remarkable differences in fossil assemblages from different localities are still present (Zhou et al., 2005). A somewhat similar assemblage has been reported from the Mesoproterozoic Kheinjua Formation in Central India and the Mesoproterozoic-Neoproterozoic Deoban Limestone in Garhwal Himalaya, but here *Eoentophysalis*, not *Myxococcoides*, is dominant (Kumar and Srivastava, 1992; 1995). Given the sparsity of analyzed assemblages from these granular phosphorites, it is difficult to ascertain to what extent these different assemblages are particularly characteristic of post-glacial cyanobacteria-dominated microbial communities at this time. Nevertheless, the recognition of populations of abundant cyanobacteria preserved in the phosphatic granules from Yichang suggests that these microorganisms were thriving, and probably, dominating in the original microbial community. The presence of abundant stromatolitic phosphorites in the Doushantuo Formation (Xue et al., 1996; Shen et al., 2000) also lends support to the possibility of pronounced bloom of oxygenic photosynthetic microbial life.

The origin of metazoans during Ediacaran time is indicated by discoveries of putative animal embryos (Xiao et al., 1998; Chen et al., 2004) and ctenophores (Zhu et al., 2008) from the

Doushantuo Formation. However, all these fossils occur in horizons around 580 Ma or younger which postdate the Gaskiers glaciation. Although Yin et al. (2007) reported large acanthomorphic acritarchs with embryo-like internal structures from the lower part of Doushantuo Formation, their relation to crown-group metazoans remains unclear. In general the putative animal fossils do not act to constrain depositional conditions and they do not constrain the possibility that a cyanobacteria-dominated ecosystem would have existed in the Taopinghe Basin during the earliest Doushantuo period.

5.3 Accelerated phosphorus cycles and phosphogenesis in the terminal Proterozoic

5.3.1 Accelerated phosphorus cycles triggered by post-glacial weathering of continental crust

The ultimate source of phosphorus in the oceans is from the weathering of continental crust which can be significantly enhanced during periods of major climate change. Although Cook (1992) argued against a phosphogenesis-glaciation link for the Proterozoic phosphorites on the basis of an outdated chronostratigaphic framework, many others have speculated that increased continental weathering rates following major glaciations have promoted an increase in riverine delivery of phosphate, which over time would have led to the accumulation of phosphorites (e.g., Papineau, 2010). In many phosphorus mines in Yichang, including Taopinghe and Zhangcunping, occurrence of major phosphorus-bearing horizons started within 5 meters above the base of the Doushantuo Formation, which immediately overlies the glacial deposits of the Nantuo Formation (Zhou et al., 2005; Liu et al., 2009). Furthermore, phosphorus-bearing rocks were observed immediately above the cap dolostone elsewhere in South China, including Weng'an (ca 550 km SW of Yichang) (Xiao et al., 2012), and Mianxian (ca 520 km NW of Yichang) (Xiao and Knoll, 2000). Thus, both stratigraphy and lithology appear to support a genetic link between glaciation/deglaciation and phosphogenesis. Intense chemical weathering triggered by extreme greenhouse conditions after the Marinoan glaciation might have resulted in the wide occurrence

of cap carbonates (Kennedy, 1996; Hoffman et al., 1998; Och and Shields-Zhou, 2012) and, subsequently, accelerated global phosphorus cycling.

As a well known feature of the South China craton, the widespread Neoproterozoic magmatic rocks (e.g., Li et al., 2003) are expected to be a major source of oceanic phosphorus. High atmospheric temperature and high CO_2 level (i.e., low pH) following the "Snowball Earth" (Hoffman et al., 1998) likely have promoted mobilization of phosphorus in the newly-formed magmatic rocks and elevated flux of nutrients to the oceans which triggered cyanobacterial blooms.

5.3.2 Role of microorganisms in transporting and concentrating phosphorus

Deposition of the Doushantuo Formation began immediately after the Marinoan Glaciation that ended at around 635 Ma (Condon et al., 2005). After deposition of the cap dolostone which is only a few meters thick and lasted less than 3 Ma, a 20~30 m-thick black shale-phosphorite sequence formed in the Yangtze Gorges and adjacent areas. Although phosphate-bearing rocks appear to be present only in shallow water environments, black shales occur throughout the Ediacaran Yangtze basin, even within the carbonate shelf. Many lines of evidence suggest that the phosphorus-bearing Doushantuo Formation formed in a restricted intra-shelf basin (Jiang et al., 2011) in which stratified water column developed (e.g., Ader et al., 2009; Li et al., 2010). Paleogeographic reconstructions of the Doushantuo Formation have shown that enriched phosphorite ore deposits are either distributed in the proximal side or in the distal side of the shelf lagoon whereas rare deposits are found in the open-ocean side of the shelf, which was invoked to argue against a upwelling P source for the Doushantuo case (Jiang et al., 2011).

While an upwelling mechanism remains elusive, biological processing, instead, provides an alternative mechanism for transporting and concentrating phosphorus in the ocean. It is widely accepted that the direct source of phosphate in sedimentary phosphorites is from the microbial

breakdown of buried organic matter and redox-driven phosphate desorption from iron and manganese oxyhydroxides (Föllmi, 1996). Sulfur isotopes of framboidal pyrite and organic biomarkers from modern phosphorites have confirmed the important role that microbial sulfate reduction (MSR) plays in the formation of modern phosphatic sediments from the Peruvian and California coast (Arning et al., 2009; Berndmeyer et al., 2012). Sulfide-oxidizing bacteria that metabolize polyphosphates are also known to release orthophosphate into pore waters where it accumulates and leads to the precipitation of apatite under anoxic conditions (Schulz & Schulz, 2005; Goldhammer et al., 2010; Brock & Schulz-Vogt, 2011). When orthophosphate is available in pore waters, some bacteria can influence phosphogenesis with the precipitation of authigenic phosphate minerals, which can cause self-phosphatization where the cells become entombed in apatite preserving detailed intracellular structures and other morphological structures (Benzerara et al., 2004; Raff et al., 2008).

Prior to these processes, scavenging of P from the oceanic waters by cyanobacteria and its subsequent sinking has brought the riverine P to the sea floor and presents an important step in the P cycling. Furthermore, our recent study of the Doushantuo granular phosphorites suggest that cyanobacteria and associated EPS might have promoted aggregated granule growth and provided nucleation templates for apatite crystallization (She et al., 2013). If this is the case, massive accumulation of phosphorites during the Doushantuo period requires excess accumulation of phosphorous, a situation that would have been accommodated by large-scale blooms of cyanobacteria, which is supported by our observation. Moreover, the carbon isotope composition of organic carbon in the phosphorites, black shales and dolostones is consistent with CO_2 fixation by photoautotrophs utilizing Rubisco and the C3 pathway. In modern oceanic waters, picoplankton can account for as much as 50% of the primary production (Dawes, 1998). In many modern coastal systems, in particular, primary production is almost entirely a function of the phytoplankton (Dawes, 1998). During the Precambrian, prior to the origin of diatoms,

coccolithophorids and modern dinoflagellates, oceanic primary productivity must have been controlled by cyanobacteria.

5.3.3 Further concentration of phosphorus through Fe-redox pumping

Redox-mediated iron-phosphate cycling (Fe-redox pumping) has been shown to be an effective phosphate trap at the redoxcline in the Black Sea (Shaffer, 1986) and was considered as an important factor in both modern and Precambrian phosphorus cycles (Heggie et al., 1990; Nelson et al., 2010). Phosphorus released from organic matter in the interfacial sediments is adsorbed onto Fe-oxyhydroxides in oxic conditions, and is subsequently released from Fe-oxyhydroxides in anoxic bottom waters. The escape of phosphate out of the sediment is prevented by re-adsorption of phosphate onto Fe-oxyhydroxides just above this redox interface. Phanerozoic phosphorite forms across the entire shelf because the ocean bottom is generally well oxygenated, providing ideal conditions for Fe-redox pumping (Nelson et al., 2010) which generally operates within the sediment pore waters (Heggie, et al., 1990). Precambrian phosphorites, however, accumulate only in shallow environment, which reflects distinct oxygenation state of the seafloor (Nelson et al., 2010).

Although Fe-redox pumping provides an effective mechanism for the concentration of phosphorus, it alone does not explains how phosphorites eventually formed as it literally prevents the precipitation of phosphate. On the other hand, despite the ability of precipitating calcium phosphate (She et al., 2013), cyanobacteria alone does not easily form phosphorites without high phosphate concentration and therefore, upwelling of deep P-rich waters is often invoked in models of phosphogenesis (Föllmi, 1996, and references therein). A combination of these two models could explain the terminal Proterozoic phosphogenesis in the Doushantuo environment.

It is widely accepted that a redox stratified shallow water column likely persisted in the Doushantuo basin (e.g., Ader et al., 2009; Li et al., 2010). The coupling and decoupling of Fe and

P in oxic and anoxic waters lead to the concentration of P below the chemocline. Moreover, it has been noted that spatial and temporal chemocline instability probably occurred in the Doushantuo basin (Shen et al., 2000; Jiang et al., 2008), which probably resulted in the upward and downward migration of P-enriched waters. The presence of a ferruginous layer in shallow ocean waters (Li et al., 2010; Xiao et al., 2012) may have further enhanced the cycling and concentration of P. In the immediate aftermath of the Marinoan glaciation, high primary productivity caused by postglacial influx of nutrients might have led to consumption of oxygen in the shallow ocean and, consequently, the upward fluctuation of chemocline. This, in turn, could have caused the upward migration of P-enriched waters with cyanobacterial EPS rapidly scavenging the phosphorus and granularization and phosphatization ensuing during syngenesis and early diagenesis.

5.3.4 A phosphogenic model

On the basis of our current knowledge of ocean chemistry and paleogeography of the Doushantuo Formation, we propose a model of terminal Proterozoic phosphogenesis (Fig. 10). In a redox-stratified intra-shelf basin, massive accumulation of phosphorites resulted from post-glacial accelerated phosphorus cycles, which include 1) an increase in riverine delivery of phosphate into the shallow ocean related to enhanced chemical weathering of continental crust (Föllmi et al., 2009), 2) rapid scavenging of phosphorus by blooming cyanobacteria (e.g., Burut-Archanai et al., 2013) followed by "organic rain", 3) remineralization of organic phosphorus through enhanced microbial anaerobic heterotrophy (e.g., bacterial sulfate reduction with increased sulfate availability) along margins of the Doushantuo shelf lagoon (Li et al., 2010; Jiang et al., 2011), 4) concentration of phosphorus near the chemocline by Fe-redox pumping (Shen et al., 2000; Cosmidis et al., 2014), and 5) upward migration of P-enriched waters caused by upwelling (Föllmi, 1996) or upward fluctuation of the chemocline and rapid precipitation of phosphate and massive accumulation of phosphorites mediated by cyanobacterial EPS (extra-

cellular polymeric substances) (She et al., 2013). This model explains both the spatial and temporal distribution of phosphorites in the Doushantuo basin. As is shown in Fig. 10, the proximal and the distal side of the shelf lagoon are the most plausible sites for phosphogenesis. Below the chemocline, degradation of the deposited organic matter led to the release of organic matter (OM) -bound phosphorus which was concentrated below the chemocline. The pulsed oxygenation of the atmosphere and shallow oceanic waters (McFadden et al., 2008) led to the variation of the chemocline and formation of the repeated cycles of black shale-granular phosphorite which characterize the lower part of the Doushantuo Formation.

In summary, the Doushantuo granular phosphorites preserve a wealth of information that collectively suggests that oxygenic photosynthetic cyanobacteria likely bloomed shortly after the Snowball Earth and produced significant quantities of oxygen. As a result, the accumulation of atmospheric oxygen paved the way for the subsequent rise of oxygen-breathing metazoans. In this sense, phosphorus cycling bridges environmental, biological and biogeochemical changes in the latest Proterozoic and provides us with a glimpse into the eventful terminal Proterozoic world.

Conclusions

The Doushantuo granular phosphorites and associated black shales were deposited immediately after the Marinoan glaciation. Phosphatic granules display zoned internal structures often associated with microfossils. Correlated in situ micro-analyses of the texture and chemistry of the Doushantuo granular phosphorites revealed primary textures formed by the rapid growth of apatite, during which microorganisms and associated extra-cellular polymeric substances (EPS) have played vital roles (She et al., 2013). Mapping of about 700 microfossils or microfossil colonies in a single thin section illustrates the high abundance of microfossils despite considerable degradation. Main microfossil types include colonies of simple spheroid *Myxococcoides*, encapsulated colonial spheroids *Eoentophysalis*, non-septate sheaths

Eomycetopsis and *Gunflintia*, and helically coiled filaments *Obruchevella* and *Heliconema*. The size, shape, community composition, and the growth patterns of the microfossils, as well as the carbon isotopic compositions of the rocks, support a cyanobacterial affinity for most microorganisms. Raman micro-spectroscopy data provides useful demonstration that 1) finely disseminated organic matter systematically occur in apatite, 2) most microfossils are composed of organic matter, 3) some microfossils are composed of pyrite mixed with organic matter, and 4) the spectra are consistent with the low metamorphic grade, which is useful to discuss microfossil taphonomy. The abundance and distribution patterns of microfossils suggest that a cyanobacteria-dominated ecosystem might have existed in the Doushantuo Basin. The occurrence of major phosphorus-bearing horizons within 5 meters above the base of the Doushantuo Formation supports a genetic link between deglaciation and phosphogenesis.

A new model is proposed to envisage the terminal Proterozoic phosphogenesis, which explains both the spatial and temporal distribution of phosphorites in the Doushantuo Basin. In a redox-stratified intra-shelf basin, accumulation of phosphorites resulted from post-glacial accelerated phosphorus cycles. Enhanced chemical weathering of continental crust led to an increase in riverine delivery of phosphate into the shallow ocean, which might have triggered the acceleration of marine biogeochemical cycles. Subsequent cyanobacterial blooms led to rapid scavenging of phosphorus which was remineralized through microbial sulfate reduction. Phosphorus was then concentrated near the chemocline by Fe-redox pumping. Finally, rapid precipitation of phosphate and accumulation of granular phosphorites were mediated by cyanobacterial EPS. Fluctuations of the chemocline led to the formation of the repeated cycles of black shale-granular phosphorite which characterizes the lower part of the Doushantuo Formation. The feedbacks between enhanced continental weathering, cyanobacterial blooms, accelerated phosphorus cycling and carbon burial thus controlled the terminal Proterozoic marine biogeochemical changes and phosphogenesis.

Acknowledgements

This work was supported by National Natural Science Foundation of China (grants 41272038 and 40802018), Fundamental Research Funds for National Universities, China University of Geosciences (Wuhan), and the 111 Program for the Ministry of Education of China and the State Administration of Foreign Expert Affairs of China (grant B07039). DP acknowledges support from the University College London, Boston College, the Carnegie Institution of Washington, NASA (the Astrobiology Institute and the Exobiology and Evolutionary Biology Program; grant numbers NNA04CC09A, NNX08AO16G, NNA09DA81A, and NNX12AG14G), and the Fond Québécois pour la Recherche sur la Nature et les Technologies. We would also like to thank Longkang Sang, Roger Mason and Xia Wen for their help in field work, and Jianhua Zhang, Zhaowei Lv, and many others in the Taopinghe mine for amicably granting us access for sample collection.

Figure captions

Fig.1 Slabs of the studied phosphorites, black shales and dolostone. Scales are shown by rulers (in mm). Dashed circles indicate the locations of drill pits from where powders were extracted and analyzed for carbon isotopes. Total organic carbon (TOC) contents and $\delta^{13}C$ (VPDB) values of organic carbon are also shown.

Fig. 2 Mapping of microfossils in a selected area (~2.3 cm^2) on thin section TP0901S with different symbols showing locations of each type of microfossil. (a) *Myxococcoides* (219 counts, 31.4%), (b) *Eoentophysalis* (13 counts, 1.9%), (c) *Gloeodiniopsis* (5 counts, 0.7%), (d) degraded *Myxococcoides* (127 counts, 18.2%), (e) *Eomycetopsis* (58 counts, 8.3%), (f) *Gunflintia* (50 counts, 7.2%), (g) possible green algae (33 counts, 4.7%), (h) *Obruchevella* (45 counts, 6.4%), (i) *Heliconema* (5 counts, 0.7%), (j) unnamed thin (width < 0.5 μm) filaments (14 counts, 2.0%), (k) degraded filaments (129 counts, 18.5%). Insect shows the relative abundance of microfossil morphotypes. (For interpretation of reference to color in this figure legend, the reader is referred to the web version of this article.)

Fig. 3 *Myxococcoides* and comparison with reported fossils. (a-c) Colonies of *Myxococcoides minor* from the Taopinghe phosphorites. (a) An example of most commonly observed colony of *Myxococcoides minor*. (b) Densely-packed *Myxococcoides* setting in darkish mucilaginous francolite matrix. (c) Possible cell division (arrow). (d) *Myxococcoides minor* from the Chichkan Formation, South Kazakhstan (Sergeev and Schopf, 2010).

Fig. 4 Histograms showing the abundance of different microfossil morphotypes in thin section TP0901S (A) and cell size distribution of *Myxococcoides* (B). Symbols in A): a, *Myxococcoides*; b, *Eoentophysalis*; c, *Gloeodiniopsis*; d, Degraded *Myxococcoides*; e, Possible green algae; f, *Eomycetopsis*; g, *Gunflintia*; h, *Obruchevella*; i, *Heliconema*; j, Unnamed thin filaments; k, Degraded filaments.

Fig. 5 Other spheroidal microfossils from the Taopinghe granular phosphorites. (a-d) Clusters of spheroidal microfossils, representing degraded variants of *Eoentophysalis*. (a) Pigmented spheroids showing internal granularization. (b-c) Spheroids with conspicuous carbonaceous cell wall, some showing multi-laminated envelopes (white arrow in b). Note the paired cells (black arrow in b and c). (d) Spheroids in tetrads (arrow and inset). (e) *Gloeodiniopsis lamellosa* (arrow and inset).

Fig. 6 Filamentous microfossils from the Taopinghe phosphorites. (a) Intertwined filaments of *Eomycetopsis*, inset showing enlarged view of the tubes. (b-c) *Gunflintia.* Dashed line in (c) shows the boundary between granule (left) and cement (right). Arrows in (c) indicate a later generation filaments that occur in early diagenetic cement. (d-e) *Obruchevella,* (e) shows a longitudinal section of *Obruchevella* (the overall brownish color is due to oil immersion). (f) loosely adjoining whorls of *Heliconema*. (g-h) Septate trichomes (green algae). (i) Transverse section of *Microcoleus*-like filaments, note the very thin "strings" which connect neighboring filaments (arrows).

Fig. 7 Microfossils showing different degrees of degradation. (a) Well-preserved *Obruchevella minor*. (b-e) *Myxococcoides* colonies with cell structures partially preserved (b), completely obscured (c), or pyritized (d-e, d: transmitted light, e: reflected light). (f) Granularization of *Eomycetopsis* and *Gunflintia*. (g) Degraded larger filaments, probably of green algae affinity.

Fig. 8 Raman images and spectra of microfossils. (a-f) Raman images showing apatite (turquoise), CM (red), quartz (blue), and poor Raman signal (black). Raman scans are made on microfossils in Fig. 5, 6 and 7: (a) from Fig. 7a, (b) from Fig. 6a, (c) from Fig. 7b, (d) from Fig. 6d, (e) from Fig. 5c, (f) from Fig. 6i. (g) Average Raman spectra of CM extracted from corresponding Raman images: (1) from (c), (2) from (a), (3) from (b), and (4) from (f). Raman spectrum of chert-hosted microfossil from Bitter Springs (Schopf et al., 2005) is also shown for comparison. (For

interpretation of reference to color in this figure legend, the reader is referred to the web version of this article.)

Fig. 9 Growth patterns of microfossils in the Taopinghe granular phosphorites. (a-b) Coccoid-dominated granule, arrows showing colony of coccoidal microfossils. Insets represent magnified view of microfossils indicated by triangles. (c-e) Filament-dominated granule. (d) Microfossils in the white square in (c), note the alternated layers of tangentially oriented (darker zone) and radially oriented filaments (lighter zone). (e) A granule occupied largely by intertwining *Eomycetopsis*. (f-g) Mixed granule (modified from She et al., 2013). (f) A zoned granule containing abundant coccoidal and filamentous microfossils. (g) Enlarged view of the area marked in (f), showing internal coccoids (triangles) and surrounding filaments (arrows). (h) A zoned granule containing randomly distributed coccoids (triangles) and filaments (arrow). (i) crossed nicols image of a granular phosphorite, the granule in the center representing the same one as is in (h).

Fig. 10 Proposed model of phosphorus cycle in the Doushantuo basin, which include 5 steps: 1) enhanced post-glacial riverine influx of P into the ocean, 2) scavenging of P by cyanobacteria and subsequent sinking of OM-bound P to the sea floor, 3) liberation of OM-bound P through microbial decomposition (e.g., MSR, microbial sulfate reduction), 4) concentration of phosphorus near the chemocline by Fe-redox pumping, and 5) upward migration of P-enriched waters caused by upwelling or upward fluctuation of the chemocline and rapid precipitation of phosphate and massive accumulation of phosphorites mediated by cyanobacterial EPS. White arrows show paths of the phosphorus cycle. (For interpretation of reference to color in this figure legend, the reader is referred to the web version of this article.)

References

Ader, M., Macouin, M., Trindade, R., Hadrien, M., Yang, Z., Sun, Z., Besse, J., 2009. A multilayered water column in the Ediacaran Yangtze platform? Insights from carbonate and organic matter paired $\delta^{13}C$. Earth and Planetary Science Letters 288, 213-227.

Allison, C.W., Awramik, S.M., 1989. Organic-walled microfossils from earliest Cambrian or latest Proterozoic Tindir Group rocks, northwest Canada. Precambrian Research 43, 253-294.

Arning, E.T., Birgel, D., Brunner, B., Peckmann, J., 2009. Bacterial formation of phosphatic laminites off Peru. Geobiology 7, 295-307.

Awramik, S.M., McMenamin, D.S., Chongyu, Y., Ziqiang, Z., Qixiu, D., Shusen, Z., 1985. Prokaryotic and eukaryotic microfossils from a Proterozoic/Phanerozoic transition in China. Nature 315, 655-658.

Bailey, J.V., Joye, S.B., Kalanetra, K.M., Flood, B.E., Corsetti, F.A., 2007. Evidence of giant sulphur bacteria in Neoproterozoic phosphorites. Nature 445, 198-201.

Barghoorn, E.S., Tyler, S.A., 1965. Microorganisms from the Gunflint Chert: These structurally preserved Precambrian fossils from Ontario are the most ancient organisms known. Science 147, 563 -575.

Battison, L., Brasier, M.D., 2012. Remarkably preserved prokaryote and eukaryote microfossils within 1Ga-old lake phosphates of the Torridon Group, NW Scotland. Precambrian Research 196–197, 204-217.

Benzerara, K., Yoon, T.H., Tyliszczak, T., Constantz, B., Spormann, A.M., Brown, G.E., 2004. Scanning transmission X-ray microscopy study of microbial calcification. Geobiology 2, 249-259.

Bernard, S., Beyssac, O., Benzerara, K., 2008. Raman mapping using advanced line-scanning systems: Geological applications. Applied spectroscopy 62, 1180-1188.

Berndmeyer, C., Birgel, D., Brunner, B., Wehrmann, L.M., Jöns, N., Bach, W., Arning, E.T., Föllmi, K.B., Peckmann, J., 2012. The influence of bacterial activity on phosphorite formation in the Miocene Monterey Formation, California. Palaeogeography, Palaeoclimatology, Palaeoecology 317, 171-181.

Bristow, T.F., Kennedy, M.J., Derkowski, A., Droser, M.L., Jiang, G., Creaser, R.A., 2009. Mineralogical constraints on the paleoenvironments of the Ediacaran Doushantuo Formation. Proceedings of the National Academy of Sciences 106, 13190-13195.

Brock, J., Schulz-Vogt, H.N., 2011. Sulfide induces phosphate release from polyphosphate in cultures of a marine Beggiatoa strain. The ISME Journal 5, 497-506.

Burut-Archanai, S., Eaton-Rye, J.J., Incharoensakdi, A., Powtongsook, S., 2013. Phosphorus removal in a closed recirculating aquaculture system using the cyanobacterium Synechocystis sp. PCC 6803 strain lacking the SphU regulator of the Pho regulon. Biochemical Engineering Journal 74, 69-75.

Chen, J., Bottjer, D.J., Oliveri, P., Dornbos, S.Q., Gao, F., Ruffins, S., Chi, H., Li, C., Davidson, E.H., 2004. Small bilaterian fossils from 40 to 55 million years before the Cambrian. Science 305, 218-222.

Condon, D., Zhu, M., Bowring, S., Wang, W., Yang, A., Jin, Y., 2005. U-Pb ages from the Neoproterozoic Doushantuo formation, China. Science 308, 95-98.

Cook, P.J., 1992. Phosphogenesis around the Proterozoic-Phanerozoic transition. Journal of the Geological Society 149, 615-620.

Cook, P.J., Shergold, J.H., 1984. Phosphorus, phosphorites and skeletal evolution at the Precambrian-Cambrian boundary. Nature 308, 231–236.

Cosmidis, J., Benzerara, K., Gheerbrant, E., Estève, I., Bouya, B., Amaghzaz, M., 2013. Nanometer-scale characterization of exceptionally preserved bacterial fossils in Paleocene phosphorites from Ouled Abdoun (Morocco). Geobiology 11, 139-153.

Cosmidis, J., Benzerara, K., Morin, G., Busigny, V., Lebeau, O., Jézéquel, D., Noël, V., Dublet, G., Othmane, G., 2014. Biomineralization of iron-phosphates in the water column of Lake Pavin (Massif Central, France). Geochimica et Cosmochimica Acta 126, 78-96.

Couradeau, E., Benzerara, K., Gérard, E., Moreira, D., Bernard, S., Brown, G.E., López-García, P., 2012. An early-branching microbialite cyanobacterium forms intracellular carbonates. Science 336, 459-462.

Dawes, C.J., 1998. Marine botany, second edition. Wiley, New York.

Föllmi, K.B., 1996. The phosphorus cycle, phosphogenesis and marine phosphate-rich deposits. Earth-Science Reviews 40, 55-124.

Föllmi, K.B., Hosein, R., Arn, K., Steinmann, P., 2009. Weathering and the mobility of phosphorus in the catchments and forefields of the Rhône and Oberaar glaciers, central Switzerland: implications for the global phosphorus cycle on glacial - interglacial timescales. Geochimica et Cosmochimica Acta 73, 2252-2282.

Fuchs, G., Thauer, R., Ziegler, H., Stichler, W., 1979. Carbon isotope fractionation by Methanobacterium thermoautotrophicum. Archives of Microbiology 120, 135-139.

Goldhammer, T., Brüchert, V., Ferdelman, T.G., Zabel, M., 2010. Microbial sequestration of phosphorus in anoxic upwelling sediments. Nature Geoscience 3, 557-561.

Heggie, D.T., Skyring, G.W., O Brien, G.W., Reimers, C., Herczeg, A., Moriarty, D.J.W., Burnett, W.C., Milnes, A.R., 1990. Organic carbon cycling and modern phosphorite formation on the East Australian continental margin: an overview. In: A.J.G. Notholt and I. Jarvis (Eds.), Phosphorite Research and Development. The Geological Society of London, Oxford, pp. 87 -117.

Hoffman, P.F., Kaufman, A.J., Halverson, G.P., Schrag, D.P., 1998. A Neoproterozoic Snowball Earth. Science 281, 1342-1346.

Hofmann, H.J., 1976. Precambrian microflora, Belcher Islands, Canada: significance and systematics. Journal of Paleontology 50, 1040-1073.

House, C.H., Schopf, J.W., McKeegan, K.D., Coath, C.D., Harrison, T.M., Stetter, K.O., 2000. Carbon isotopic composition of individual Precambrian microfossils. Geology 28, 707-710.

Huldtgren, T., Cunningham, J.A., Yin, C., Stampanoni, M., Marone, F., Donoghue, P.C., Bengtson, S., 2011. Fossilized nuclei and germination structures identify Ediacaran “animal embryos” as encysting protists. Science 334, 1696-1699.

Jiang, G., Kennedy, M.J., Christie-Blick, N., Wu, H., Zhang, S., 2006. Stratigraphy, sedimentary structures, and textures of the Late Neoproterozoic Doushantuo cap carbonate in South China. Journal of Sedimentary Research 76, 978 -995.

Jiang, G., Shi, X., Zhang, S., Wang, Y., Xiao, S., 2011. Stratigraphy and paleogeography of the Ediacaran Doushantuo Formation (ca. 635-551 Ma) in South China. Gondwana Research 19, 831-849.

Jiang, G., Zhang, S., Shi, X., Wang, X., 2008. Chemocline instability and isotope variations of the Ediacaran Doushantuo basin in South China. Science in China Series D: Earth Sciences 51, 1560-1569.

Kennedy, M.J., 1996. Stratigraphy, sedimentology, and isotopic geochemistry of Australian Neoproterozoic postglacial cap dolostones: deglaciation, $\delta^{13}C$ excursions, and carbonate precipitation. Journal of Sedimentary Research 66, 1050-1064.

Kirschvink, J.L., Gaidos, E.J., Bertani, L.E., Beukes, N.J., Gutzmer, J., Maepa, L.N., Steinberger, R.E.,

2000. Paleoproterozoic snowball Earth: Extreme climatic and geochemical global change and its biological consequences. Proceedings of the National Academy of Sciences 97, 1400-1405.

Knoll, A.H., 1982. Microfossils from the late Precambrian Draken Conglomerate, Ny Friesland, Svalbard. Journal of Paleontology 56, 755-790.

Knoll, A.H., Strother, P.K., Rossi, S., 1988. Distribution and diagenesis of microfossils from the lower Proterozoic Duck Creek Dolomite, Western Australia. Precambrian Research 38, 257-279.

Knoll, A.H., Swett, K., Mark, J., 1991. Paleobiology of a Neoproterozoic tidal flat/lagoonal complex: the Draken Conglomerate Formation, Spitsbergen. Journal of Paleontology 65, 531-570.

Kumar, S., Srivastava, P., 1992. Middle to Late Proterozoic microbiota from the Deoban Limestone, Garhwal Himalaya, India. Precambrian Research 56, 291-318.

Kumar, S., Srivastava, P., 1995. Microfossils from the Kheinjua Formation, Mesoproterozoic Semri Group, Newari area, central India. Precambrian Research 74, 91-117.

Li, C., Love, G.D., Lyons, T.W., Fike, D.A., Sessions, A.L., Chu, X., 2010. A stratified redox model for the Ediacaran ocean. Science 328, 80-83.

Li, X., Li, Z., Ge, W., Zhou, H., Li, W., Liu, Y., Wingate, M.T.D., 2003. Neoproterozoic granitoids in South China: crustal melting above a mantle plume at ca. 825 Ma? Precambrian Research 122, 45-83.

Liu, P.J., Yin, C.Y., Gao, L.Z., Tang, F., Chen, S.M., 2009. New material of microfossils from the Ediacaran Doushantuo Formation in the Zhangcunping area, Yichang, Hubei Province and its zircon SHRIMP U-Pb age. Chinese Science Bulletin 54, 1058-1064.

McArthur, J.M., Coleman, M.L., Bremner, J.M., 1980. Carbon and oxygen isotopic composition of structural carbonate in sedimentary francolite. Journal of the Geological Society 137, 669-673.

McFadden, K.A., Huang, J., Chu, X., Jiang, G., Kaufman, A.J., Zhou, C., Yuan, X., Xiao, S., 2008. Pulsed oxidation and biological evolution in the Ediacaran Doushantuo Formation. Proceedings of the National Academy of Sciences 105, 3197.

McFadden, K.A., Xiao, S., Zhou, C., Kowalewski, M., 2009. Quantitative evaluation of the biostratigraphic distribution of acanthomorphic acritarchs in the Ediacaran Doushantuo Formation in the Yangtze Gorges area, South China. Precambrian Research 173, 170-190.

Monty, C.L.V., 1976. The Origin and Development of Cryptalgal Fabrics. In: M.R. Walter (Ed.),

Stromatolites. Developments in sedimentology. Elsevier, Amsterdam, pp. 193-249.

Nelson, G.J., Pufahl, P.K., Hiatt, E.E., 2010. Paleoceanographic constraints on Precambrian phosphorite accumulation, Baraga Group, Michigan, USA. Sedimentary Geology 226, 9-21.

Och, L.M., Shields-Zhou, G.A., 2012. The Neoproterozoic oxygenation event: environmental perturbations and biogeochemical cycling. Earth-Science Reviews 110, 26-57.

Papineau, D., 2010. Global biogeochemical changes at both ends of the Proterozoic: insights from phosphorites. Astrobiology 10, 165-181.

Papineau, D., DeGregorio, B.T., Stroud, R.M., Steele, A., Pecoits, E., Konhauser, K., Wang, J., and Fogel, M.L., 2010. Ancient graphite in the Eoarchean quartz-pyroxene rock from Akilia in southern West Greenland II: Isotopic and chemical compositions and comparison with Paleoproterozoic banded iron formations. Geochimica et Cosmochimica Acta **74**, 5884-5905.

Papineau, D., De Gregorio, B.T., Cody, G.D., O Neil, J., Steele, A., Stroud, R.M., Fogel, M.L., 2011. Young poorly crystalline graphite in the > 3.8-Gyr-old Nuvvuagittuq banded iron formation. Nature Geoscience 4, 376-379.

Raff, E.C., Schollaert, K.L., Nelson, D.E., Donoghue, P.C., Thomas, C., Turner, F.R., Stein, B.D., Dong, X., Bengtson, S., Huldtgren, T., 2008. Embryo fossilization is a biological process mediated by microbial biofilms. Proceedings of the National Academy of Sciences 105, 19360-19365.

Redfield, A.C., 1958. The biological control of chemical factors in the environment. American Scientist 46, 205-221.

Schidlowski, M., Hayes, J., Kaplan, I., 1983. Isotopic inferences of ancient biochemistries: carbon, sulfur, hydrogen, and nitrogen. In: J. Schopf (Ed.), Earth's Earliest Biosphere: Its Origin and Evolution. Princeton University Press, New Jersey, pp. 149-185.

Schopf, J.W., 1968. Microflora of the Bitter Springs Formation, late Precambrian, central Australia. Journal of Paleontology 42, 651-688.

Schopf, J.W., Kudryavtsev, A.B., Agresti, D.G., Czaja, A.D., Wdowiak, T.J., 2005. Raman imagery: a new approach to assess the geochemical maturity and biogenicity of permineralized Precambrian fossils. Astrobiology 5, 333-371.

Schulz, H.N., Schulz, H.D., 2005. Large sulfur bacteria and the formation of phosphorite. Science 307:

416-418.

Sergeev, V.N., Schopf, J.W., 2010. Taxonomy, Paleoecology and Biostratigraphy of the Late Neoproterozoic Chichkan Microbiota of South Kazakhstan: The Marine Biosphere on the Eve of Metazoan Radiation. Journal of Paleontology 84, 363-401.

Shaffer, G., 1986. Phosphate pumps and shuttles in the Black Sea. Nature 321, 515–517.

Sharma, M., Sergeev, V.N., 2004. Genesis of carbonate precipitate patterns and associated microfossils in Mesoproterozoic formations of India and Russia—a comparative study. Precambrian Research 134, 317-347.

Sharma, M., Shukla, Y., 2009. The evolution and distribution of life in the Precambrian eon-global perspective and the Indian record. Journal of Biosciences 34, 765-776.

She, Z., Strother, P., McMahon, G., Nittler, L.R., Wang, J., Zhang, J., Sang, L., Ma, C., Papineau, D., 2013. Terminal Proterozoic cyanobacterial blooms and phosphogenesis documented by the Doushantuo granular phosphorites I: *In situ* micro-analysis of textures and composition. Precambrian Research 235, 20-35.

Shen, Y., Schidlowski, M., Chu, X., 2000. Biogeochemical approach to understanding phosphogenic events of the terminal Proterozoic to Cambrian. Palaeogeography, Palaeoclimatology, Palaeoecology 158, 99-108.

Srivastava, P., 2006. Meso-Neoproterozoic coated grains and palaeoecology of associated microfossils: The Deoban Limestone, Lesser Himalaya, India. Palaeogeography, Palaeoclimatology, Palaeoecology 239, 241-252.

Strother, P.K., Tobin, K., 1987. Observations on the genus *Huroniospora* Barghoorn: Implications for paleoecology of the Gunflint microbiota. Precambrian Research 36, 323-333.

Walter, M.R., Bauld, J., Brock, T.D., 1976. Microbiology and Morphogenesis of Columnar Stromatolites (Conophyton, Vacerrilla) from Hot Springs in Yellowstone National Park. In: M.R. Walter (Ed.), Stromatolites. Developments in sedimentology. Elsevier, Amsterdam, pp. 273-310.

Xiao, S., 2004. New multicellular algal fossils and acritarchs in Doushantuo chert nodules (Neoproterozoic; Yangtze Gorges, south China). Journal of Paleontology 78, 393-401.

Xiao, S., Knoll, A.H., 2000. Phosphatized animal embryos from the Neoproterozoic Doushantuo formation

at Weng'an, Guizhou, South China. Journal of Paleontology 74, 767-788.

Xiao, S., Knoll, A.H., Yuan, X., Pueschel, C.M., 2004. Phosphatized multicellular algae in the Neoproterozoic Doushantuo Formation, China, and the early evolution of florideophyte red algae. American Journal of Botany 91, 214-227.

Xiao, S., McFadden, K.A., Peek, S., Kaufman, A.J., Zhou, C., Jiang, G., Hu, J., 2012. Integrated chemostratigraphy of the Doushantuo Formation at the northern Xiaofenghe section (Yangtze Gorges, South China) and its implication for Ediacaran stratigraphic correlation and ocean redox models. Precambrian Research 192-195, 125-141.

Xiao, S., Zhang, Y., Knoll, A.H., 1998. Three-dimensional preservation of algae and animal embryos in a Neoproterozoic phosphorite. Nature 391, 553-558.

Xiao, S., Zhou, C., Liu, P., Wang, D., Yuan, X., 2014. Phosphatized acanthomorphic acritarchs and related microfossils from the Ediacaran Doushantuo Formation at Weng'an (South China) and their implications for biostratigraphic correlation. Journal of Paleontology 88, 1-67.

Xue, Y., Tang, T., Yu, C., Zhou, C., 1996. Microfossils and phosphatization in the Doushantuo phosphate deposits. In: Ye, L. (Ed.), Aspects of Mineralization. Oceanic Press, Beijing, pp. 41-63.

Xue, Y., Zhou, C., Tang, T., 1999. “Animal embryos”, a misinterpretation of Neoproterozoic microfossils. Acta Micropalaeontologica Sinica 16, 1-4.

Yin, L., Sun, W., 1994. Microbiota from the Neoproterozoic Liulaobei Formation in the Huainan region, northern Anhui, China. Precambrian Research 65, 95-114.

Yin, L., Zhu, M., Knoll, A.H., Yuan, X., Zhang, J., Hu, J., 2007. Doushantuo embryos preserved inside diapause egg cysts. Nature 446, 661-663.

Yuan, X., Wang, Q., Zhang, Y., 1993. Late Precambrian Weng'an Biota from Guizhou, southwest China. Acta Micropalaeontologica Sinica 10, 409-420.

Zhongying, Z., 1982. Filamentous microfossils from the Doushantuo Formation (Late Sinian) of South China. Journal of Paleontology 56, 1251-1256.

Zhongying, Z., 1985. Coccoid microfossils from the Doushantuo Formation (Late Sinian) of South China. Precambrian Research 28, 163-173.

Zhou, C., Xie, G., Xiao, S., 2005. New data of microfossils from Doushantuo Formation at Zhangcunping,

Hubei Province. Acta Micropalaeontologica Sinica 22, 217-224.

Zhou, C., Yuan, X., Xiao, S., Chen, Z., Xue, Y., 2004. Phosphatized fossil assemblage from the Doushantuo Formation in Baokang, Hubei Province. Acta Micropalaeontologica Sinica 21, 349-366.

Zhu, M., Gehling, J.G., Xiao, S., Zhao, Y., Droser, M.L., 2008. Eight-armed Ediacara fossil preserved in contrasting taphonomic windows from China and Australia. Geology 36, 867-870.

Table 1

Table 1 Counted occurrences of various microfossil morphtypes and their relative abundances

Taxa	*Myxococcoides* (a) *	*Eoentophysalis* (b)	*Gloeodiniopsis* (c)	Degraded *Myxococcoides* (d)	*Eomycetopsis* (e)	*Gunflintia* (f)	Possible green algae (g)	*Obruchevella* (h)	*Heliconema* (i)	Unnamed thin filaments (j)	Degraded filaments (k)	Total
Occurrence	219	13	5	127	58	50	33	45	5	14	129	698
Proportion (%)	31.4	1.9	0.7	18.2	8.3	7.2	4.7	6.4	0.7	2.0	18.5	100.0

* One colony of *Myxococcoides* or degraded *Myxococcoides* was counted as 1 occurrence, despite the number of cells.

Table 2

Table 2 Raman spectral data of representative microfossils in the Doushantuo phosphorites

Raman scans	Microfossil morphtypes	Depth of scan (μm)	G-band position	G-band FWHM	D-band position	D-band FWHM	D-band Intensity	G-band Intensity
TP0901S_a82	Slightly degraded *Myxococcoides* in phosphorite	4	1592.6	81.0	1334.3	135.4	98	112
TP0901S_a211	Slightly degraded *Myxococcoides* in phosphorite	8.5	1600.6	83.7	1355.1	112.9	57	64
TP0901S_a73	Degraded *Myxococcoides* in phosphorite	3	1600.6	85.6	1334.3	115.7	85	91
TP0901S_01	Well preserved *Obruchevella* in phosphorite	4	1604.9	74.1	1351.1	98.2	273	381
TP0901S_12	Well preserved *Eomycetopsis* in phosphorite	7.5	1600.6	79.2	1334.3	113.2	69	81
TP0902_17	Well preserved *Eomycetopsis* in phosphorite	10	1604.6	72.6	1334.9	108.3	81	106
YG0914_03	Well preserved *Microcoleus*-like filaments in Chert	3	1613.0	34.1	1346.7	133.4	640	1447
YG0914_10	Well preserved *Microcoleus*-like filaments in Chert	3	1613.0	33.7	1355.3	133.1	79	150

Table 3

Table 3 Carbon isotope data of the Doushantuo phosphorites and associated rocks

Sample No.	Lithology	$\delta^{13}C_{TC}$	TC wt%	$\delta^{13}C_{org}$	TOC wt%	$\delta^{13}C_{IC}$*	IC wt%*
TP0901	Granular phosphorite	-10.0	0.83	-28.1	0.14	-6.3	0.69
TP0902	Granular phosphorite	-9.8	0.61	-29.1	0.04	-8.5	0.57
TP0903	Granular phosphorite	n.a.	n.a.	-28.8	0.03		
TP0908	Massive phosphorite	n.a.	n.a.	-26.0	0.02		
TP0909	Massive phosphorite	n.a.	n.a.	-27.1	0.02		
TP0911	Finely laminated black shale	n.a.	n.a.	-29.7	0.93		
TP0912	Phosphatic nodule in black shale	n.a.	n.a.	-28.6	1.15		
YG0914.a	Chert nodule in dolomicrite	-5.7	0.49	-32.9	0.48		
YG0914.b	Dolomicrite matrix	n.a.	n.a.	-27.2	0.37		
YG0914.d	Dolomicrite matrix	3.7	4.23	-26.6	0.38	6.7	3.85
YG0914.e	Dolomicrite matrix	1.8	3.54	-26.5	0.59	7.4	2.96
YG0914.f	CM-rich dolomicrite matrix	2.9	6.21	-26.8	0.78	7.1	5.44
YG0914.g	CM-rich dolomicrite matrix	1.1	6.67	-28.5	1.04	6.6	5.63

* Values calculated based on mass balance.

Figure 1

She et al_2014_Fig. 1

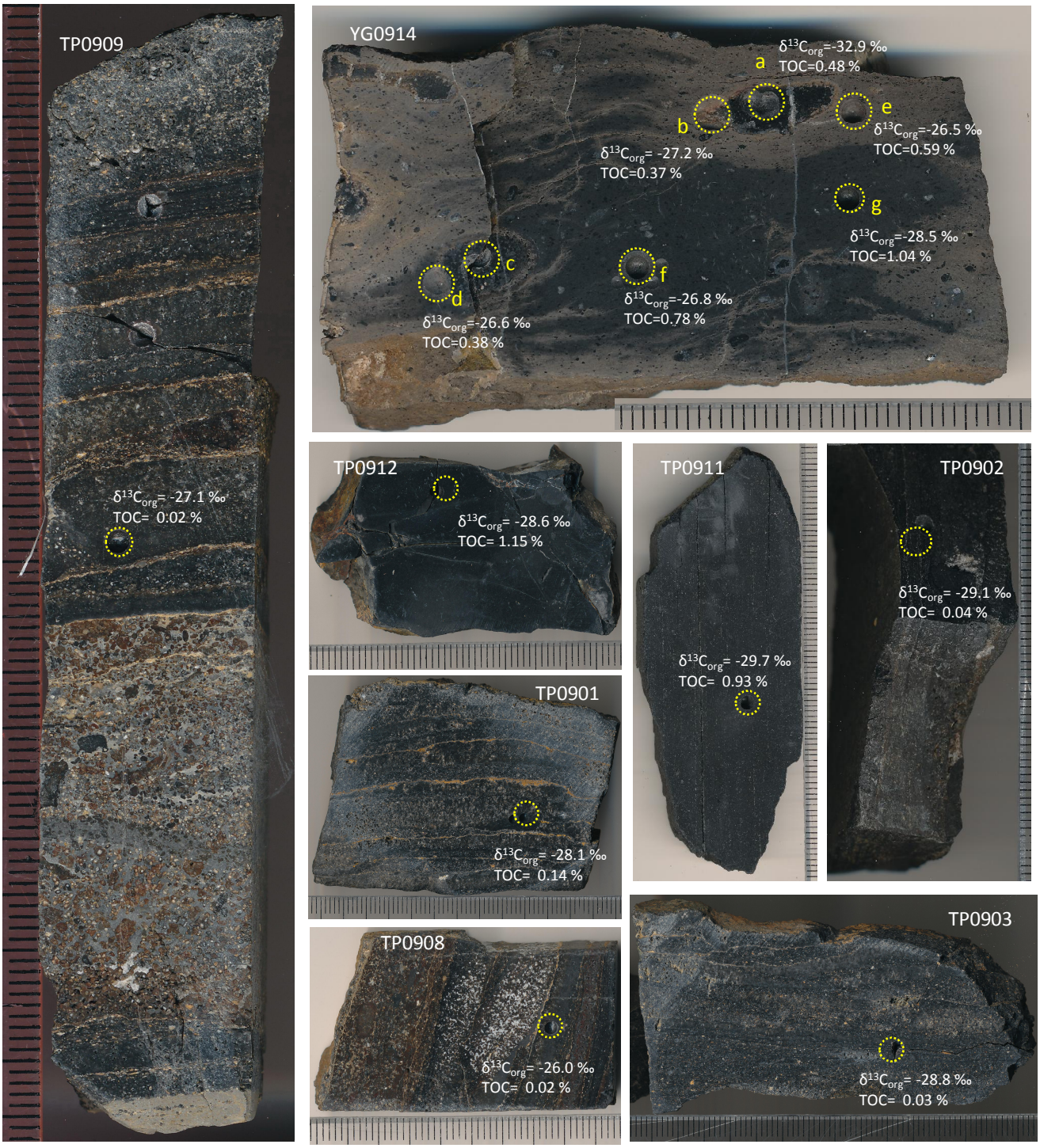

Figure 2

She et al., 2014_Fig. 2

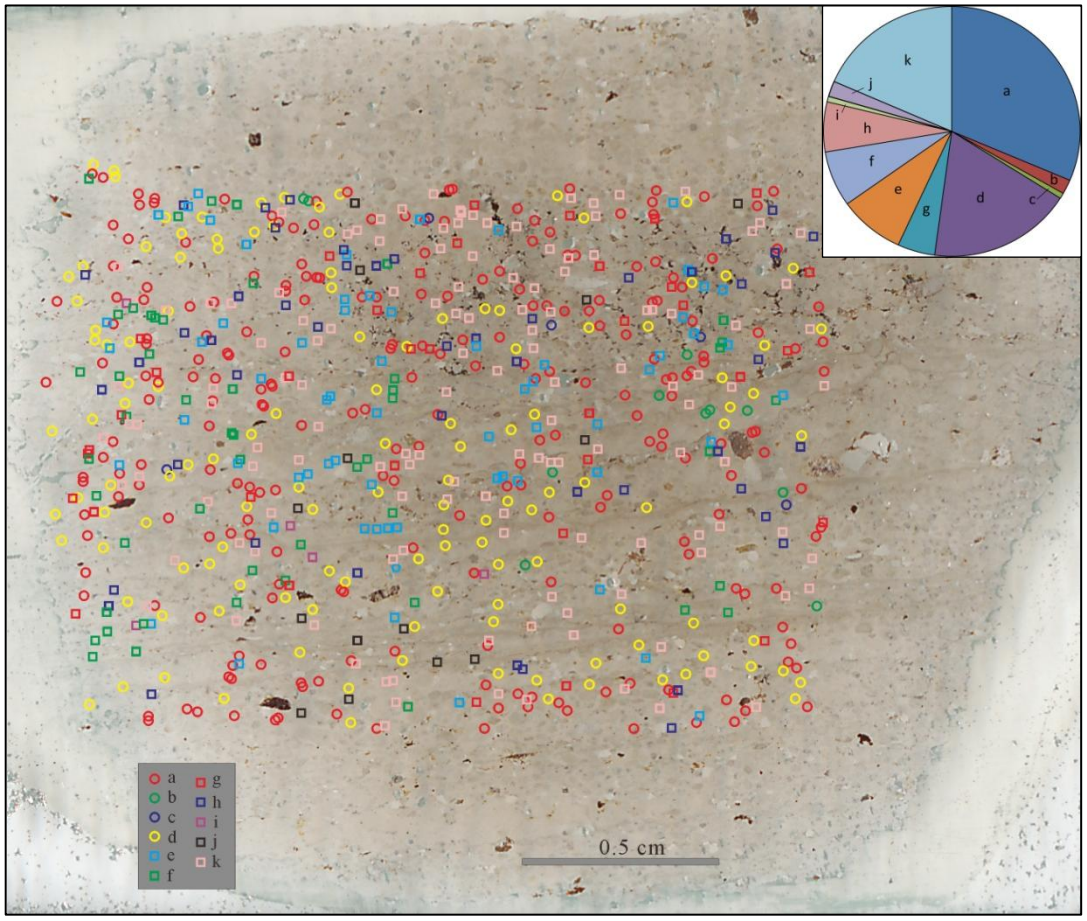

Figure 3

She et al., 2014_Fig.3

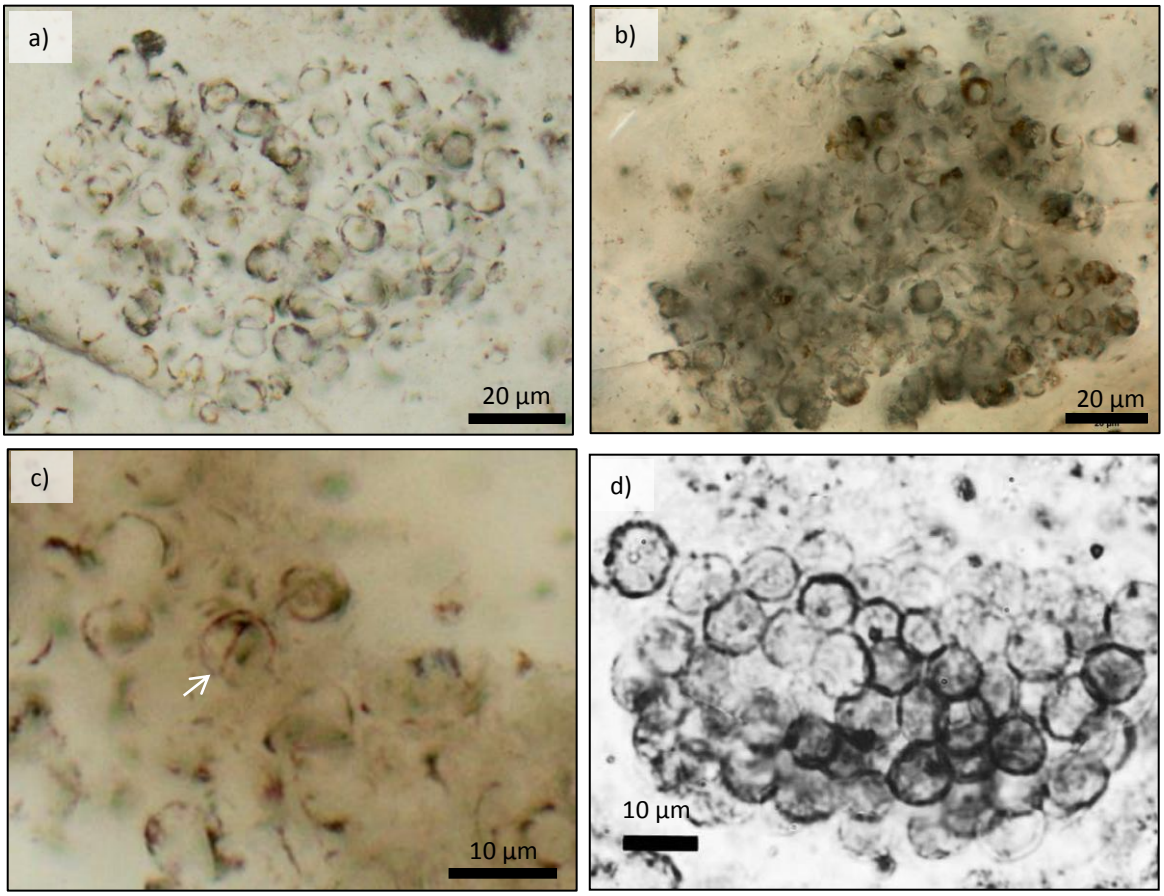

Figure 4

She et al., 2014_Fig.4

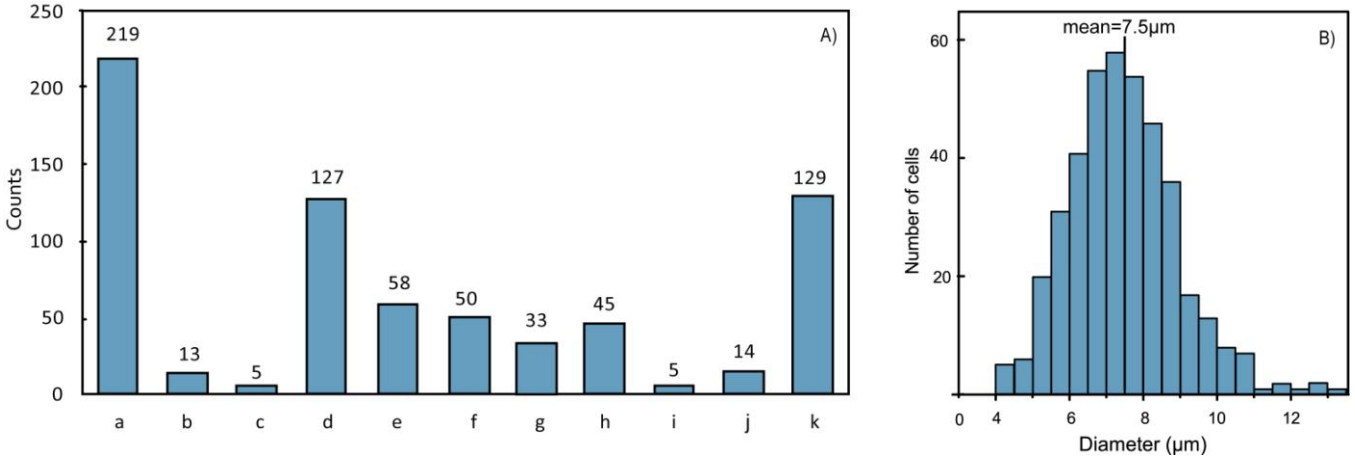

Figure 5

She et al., 2014_Fig.5

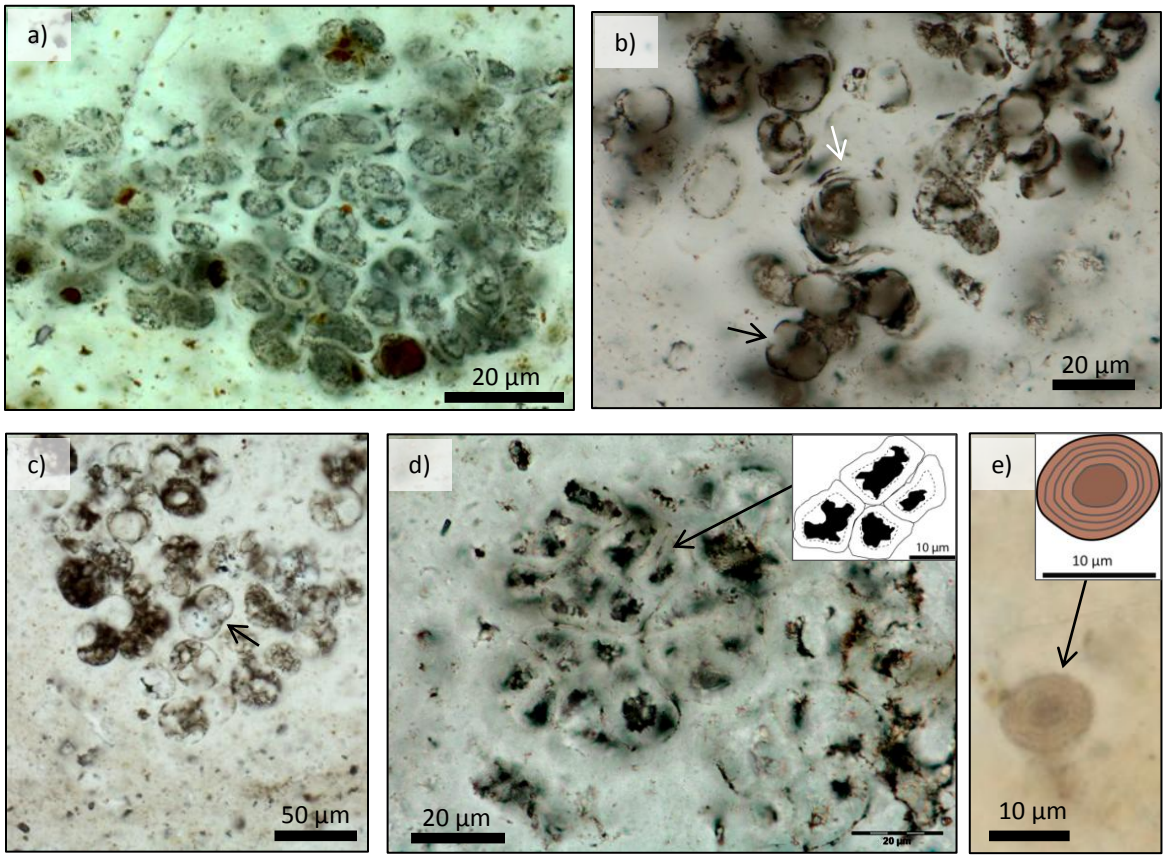

Figure 6

She et al_2014_Fig.6

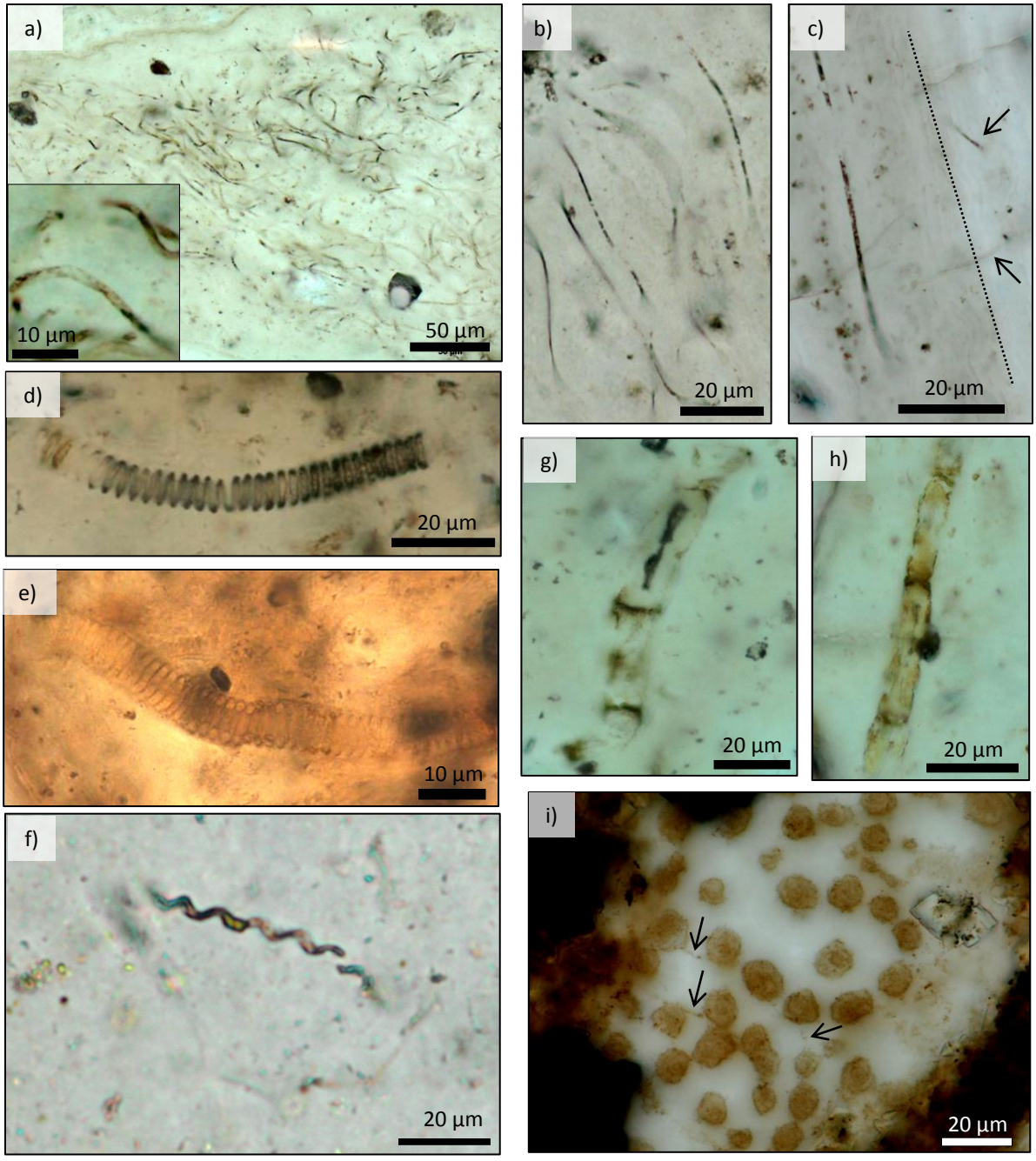

Figure 7

She et al_2014_Fig.7

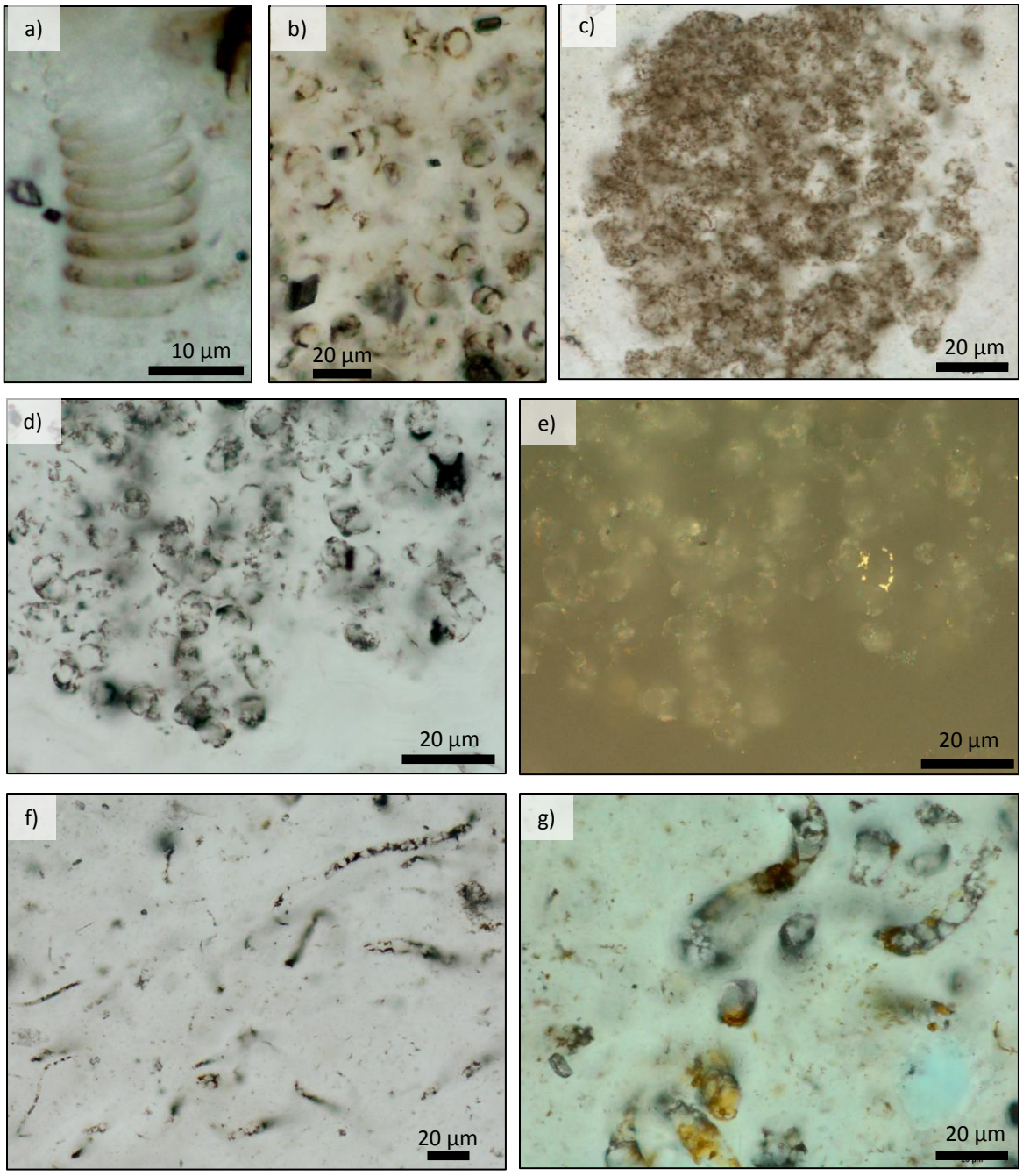

Figure 8

She et al_2014_Fig.8

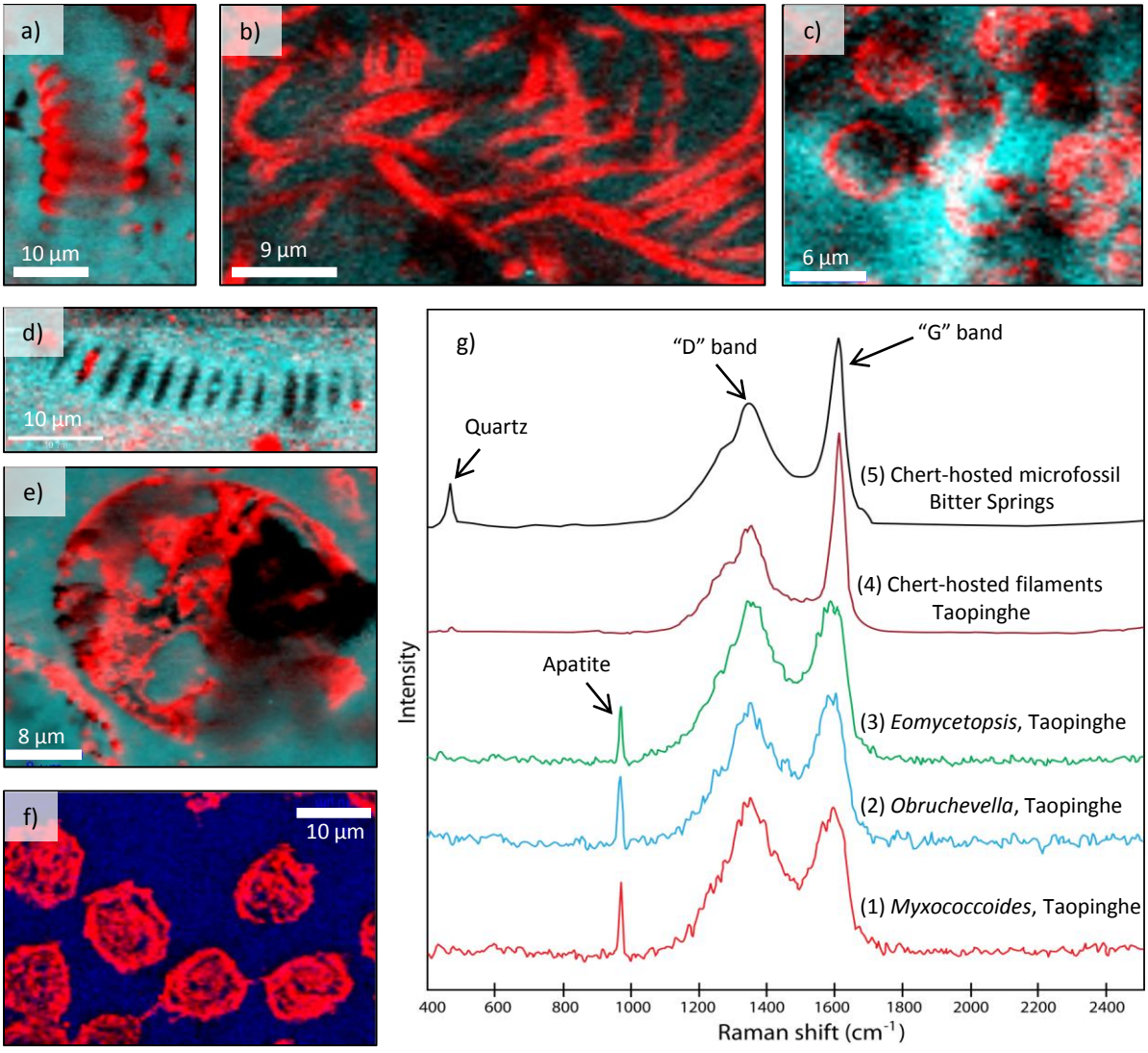

Figure 9

She et al_2014_Fig.9

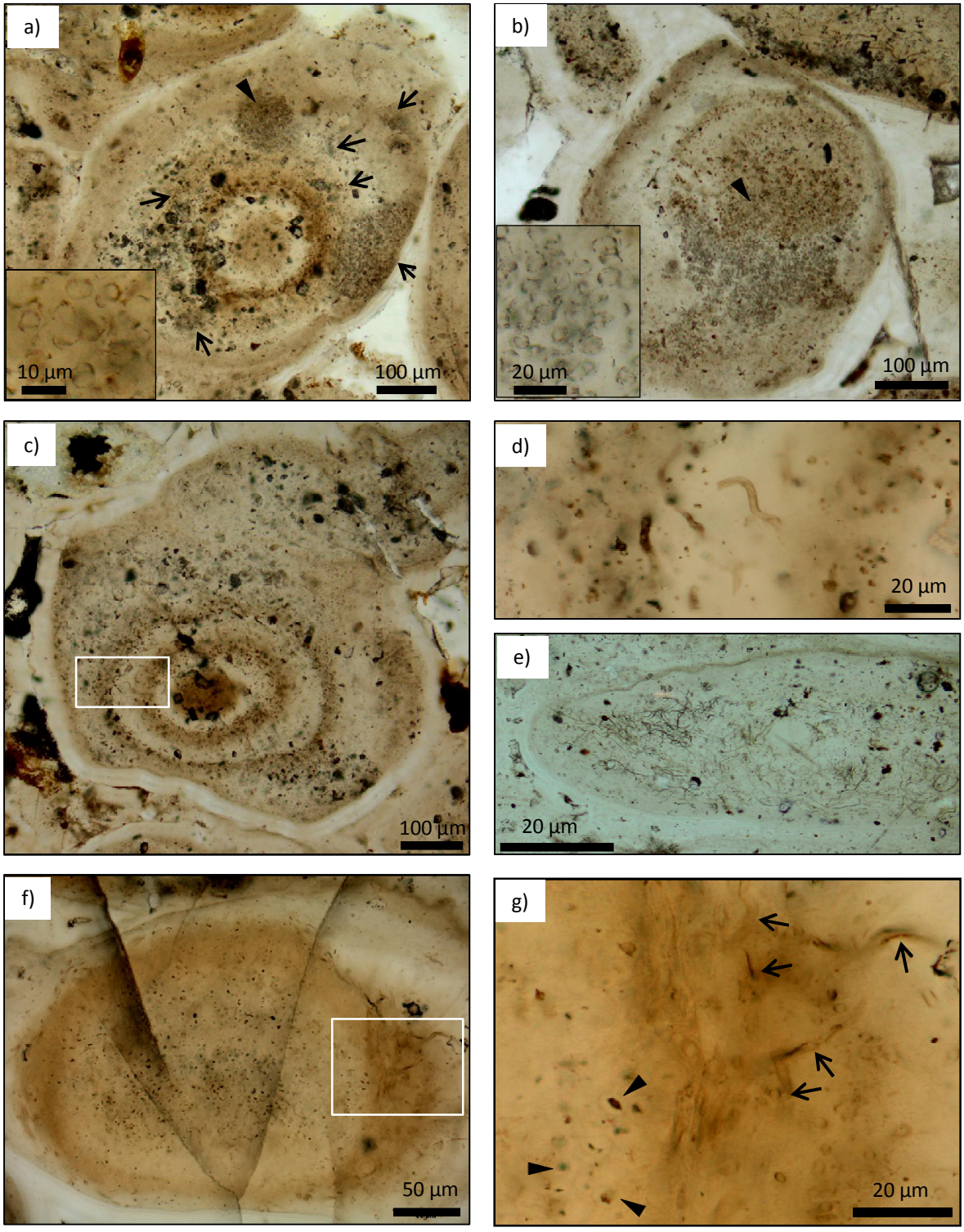

She et al_2014_Fig.9_continued

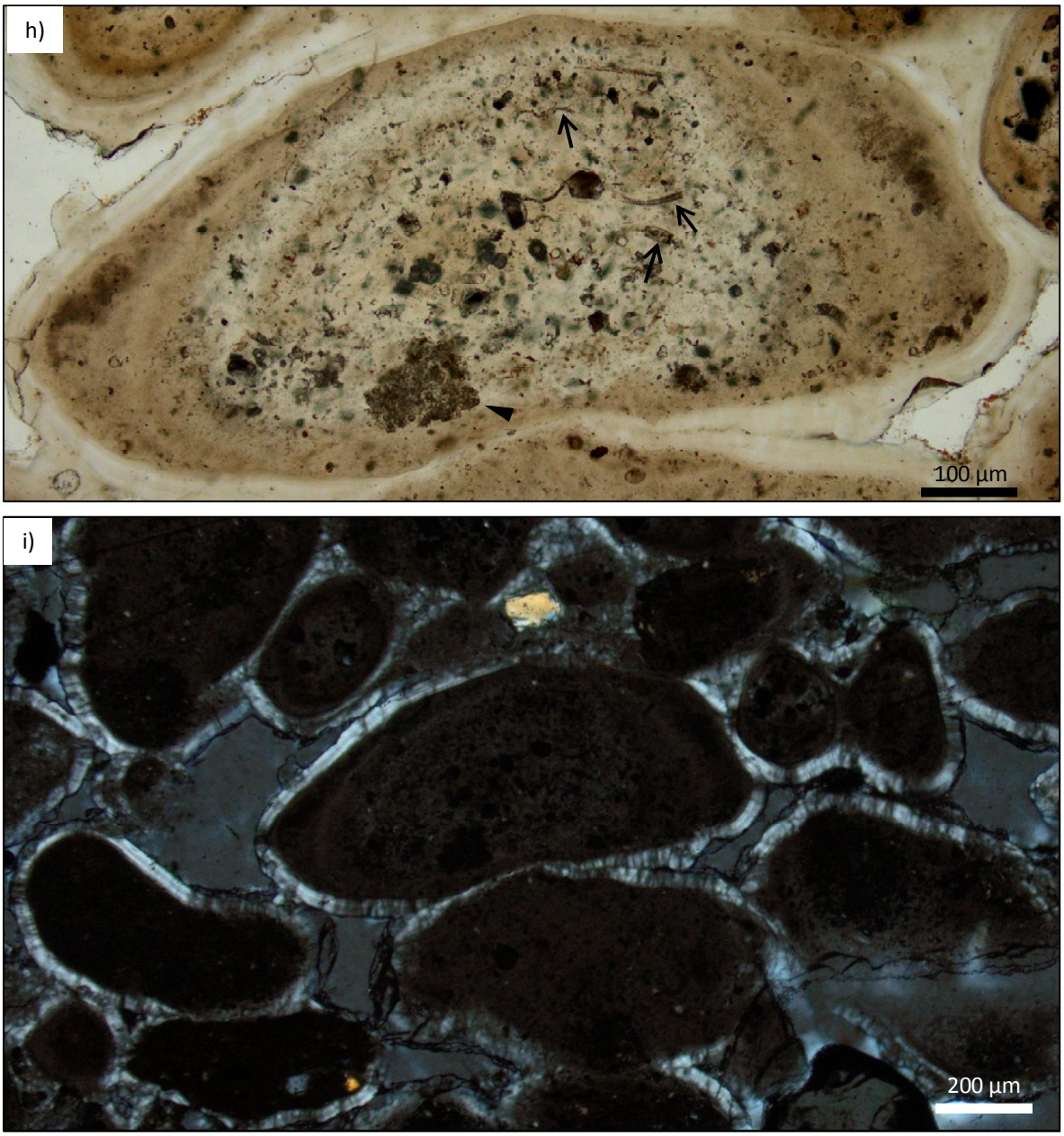

Figure 10

She et al,2014_Fig. 10